Multiphonon relaxation of moderately excited carriers in Si/SiO_{2} nanocrystals

A. S. Moskalenko, J. Berakdar, A. N. Poddubny, A. A. Prokofiev, I. N. Yassievich, and S. V. Goupalov

Multiphonon relaxation of moderately excited carriers in Si/SiO$_2$ nanocrystals

A.S. Moskalenko[*] and J. Berakdar

Institut für Physik, Martin-Luther-Universität Halle-Wittenberg,
Nanotechnikum-Weinberg, Heinrich-Damerow-Strasse 4, 06120 Halle, Germany

A.N. Poddubny,[†] A.A. Prokofiev, and I.N. Yassievich

Ioffe Physical-Technical Institute of RAS, 194021 St. Petersburg, Russia

S.V. Goupalov

Department of Physics, Jackson State University, Jackson, MS 39217, USA and
Ioffe Physical-Technical Institute of RAS, 194021 St. Petersburg, Russia

We study the phonon-assisted intraband relaxation of electrons and holes confined in Si nanocrystals. The rates of relaxation processes are calculated as functions of the nanocrystal size and of the temperature. It occurs that the main contribution to the relaxation is provided by the mechanism where a single acoustic and a number of optical phonons, which is necessary to compensate the energy difference between the quantized charge carrier levels, are involved. We show that the phonon-assisted transitions between neighboring, size-quantized levels occur typically on a picosecond timescale, but vary over several orders of magnitude with the nanocrystal size. This results in a multi-exponential decay of the carrier populations averaged over an ensemble of the nanocrystals with a given size distribution. When the nanocrystal size is reduced and more than two phonons are required for the transition, there is a qualitative difference in the behavior of the transition probabilities between the electrons and the holes. Whereas the electron transition times strongly oscillate around approximately the same mean values in the picosecond range with some drops towards nanoseconds, there is a clearly pronounced tendency of the relaxation time increase into the nanosecond time range for the hole transitions when the nanocrystal size is decreased. The increase of the temperature leads to a moderate decrease of the relaxation times but does not change the picture qualitatively.

I. INTRODUCTION

Materials based on Si nanocrystals (NCs) are considered as potential building blocks for future silicon-based photonic and photovoltaic devices[1–5] fostering an intensive investigation of their properties (see e.g. Refs. 6 and 7 for reviews). Recent observations of a very efficient blue emission from excited Si NCs on ultrafast time scale and of other short-living emission bands[5,8–10] call for a systematic description of the relaxation processes following the excitation of the non-equilibrium charge carriers in Si NCs. Excitation by light with the photon energy exceeding the optical gap of Si NCs creates mainly hot electrons and cold holes.[11] If several electron-hole pairs have been created in a NC, the Auger recombination process can contribute to the dynamics of the confined carriers on the picosecond time scale.[12,13] In the case of a moderate excitation intensity, when only one electron-hole pair can occur in a NC, the Coulomb interaction would redistribute the excess of the excitation energy between the electron and the hole due to the elastic Auger scattering leading to appearance of hot holes and establishing a joint electron-hole distribution on a subpicosecond timescale.[11,14] It is the phonon emission that controls the energy relaxation of hot carriers confined in Si NCs. We may recall that in bulk Si hot carriers can effectively thermalize due to single-phonon emission processes on subpicosecond timescales.[15–17] The space quantization of the charge carriers in Si NCs leads to discrete levels. For moderately excited carriers (excess energies $\lesssim 1$ eV), the energy spacings between neighboring levels mostly exceed the phonon energies so that the single-phonon intraband relaxation is forbidden by the energy conservation. It is clear that in this case multiphonon transitions should play an essential role in the hot carrier relaxation whereas one-phonon transitions are more important for the highly excited carrier states with smaller energy spacings.[11]

The issue of the multiphonon-induced charge carrier relaxation was investigated theoretically and experimentally for semiconductor quantum dots based on A$_3$B$_5$, A$_2$B$_6$, and A$_4$B$_6$ semiconductors.[18–22] Up to date, only few aspects of the multiphonon charge carrier relaxation in Si NCs have been addressed theoretically.[14,23] The goal of the present paper is to provide a systematic theoretical description of the multiphonon relaxation of the moderately excited carriers in the particular case of the Si NCs embedded in the SiO$_2$ matrix. Certain peculiarities (described below) can be expected in this case.

Modeling multiphonon transitions in Si NCs embedded in the SiO$_2$ matrix requires the knowledge of the charge carrier states in these NCs as well as the appropriate description of the phonons and the carrier-phonon interactions. In the past, many various models were used to calculate the charge carrier states in the Si NCs. *Ab-initio*

models are limited to very small nanocrystal sizes.[6,24–27] Semi-empirical approaches like tight-binding[6,14,28] and pseudopotential[29,30] models are a good option in the case of the free-standing or hydrogen-passivated Si NCs but they still lack an appropriate description of the Si/SiO$_2$ boundary leading to a strong overestimation of the quantization energies in the case of the Si NCs embedded in SiO$_2$. In this respect, it seems natural to employ a model based on the multiband effective mass approximation supplemented by the appropriate boundary conditions, along the lines of previous studies.[31] We model the hole spectrum in Si by the Luttinger Hamiltonian in the spherical approximation and the limit of a vanishing spin-orbit interaction.[32] The electron spectrum in Si is contributed by six equivalent Δ-valleys with an anisotropic dispersion.[33] This approach provides a reliable description of the electron and hole states in Si NCs embedded in the SiO$_2$ matrix leading to a good agreement with the experimental data on the optical gap and the electron-hole radiative recombination time.[31] It is a good approximation to neglect the effect of the spin-orbit coupling when calculating the charge carrier states in Si NCs and modeling their energy relaxation.[34] This coupling should be included when considering the spin relaxation, which is an important issue for silicon spintronics.[35] The spin relaxation in bulk silicon takes place on nanoseconds to microseconds times[34,36,37] being much longer than the typical energy relaxation times. The details of the corresponding processes are still under an active theoretical consideration even for the bulk case[37]. Thus, treatment of the spin relaxation in the case of Si NCs is clearly beyond the scope of the present work but surely would be an interesting challenge for future investigations. We will limit our consideration by a moderate excitation level of the NCs. In this case additional level splittings due to the valley-orbit interaction and to the anisotropy of the crystal structure do not significantly modify the typical energy level separations for not too small NCs.[28]

In the present study we consider the phonon spectrum and the electron-phonon interactions using the parameters of bulk Si. It was shown in Refs. 38,39 that for NCs with diameters $D \gtrsim 4$ nm the interatomic forces remain close to those in the bulk and there are no dramatic changes in the phonon spectrum. More rigorous treatment of the phonon spectrum is necessary in order to get better quantitative results for small NCs with diameters on the order of 3 nm and smaller, which is out of the scope of the present work. We notice, however, that even for small NC sizes no dramatic effects are expected.[40]

Our treatment of the multiphonon transitions is based on the Huang-Rhys model[19,32,41,42]. Some peculiarities arise when this model is applied to the relaxation of electrons and holes in Si NCs. We describe the interaction of the valence-band holes with the zone-centered optical phonons by the Bir-Pikus Hamiltonian[33,43], whereas the multiphonon transitions within the conduction band require the emission of *intervalley* optical phonons.[33] Therefore, we need to extend the Huang-Rhys model to

the case of the transitions between the degenerate levels. In the case of the electrons, where the emitted optical phonon transfers the electron to the state in the opposite valley and there is a single final state for the given initial state and the number of the emitted optical phonons, the problem is solved using a perturbative approach. For holes, there are several possibilities for the final state belonging to the degenerate multiplet. In this case we will show how the problem can be approximately reduced to the case of the nondegenerate levels. The bulk of the relaxation processes we consider are triggered by the emission or the absorption of a "promoting" acoustic phonon which assures the overall energy conservation.[32,44]. However, we also discuss the processes where only optical or several acoustic phonons are emitted.

The paper is organized as follows. In Section II we investigate the multiphonon relaxation of the valence-band holes. Section III is devoted to the phonon-assisted relaxation of the conduction-band electrons. In Section IV we summarize the results and compare the obtained relaxation rates with those for competing processes.

II. MULTIPHONON ENERGY RELAXATION OF HOLES

A. Hole size quantization

We consider the states of holes confined in a spherical Si NC in the limit of a vanishing spin-orbit splitting. In this limit the valence band in bulk Si at the Γ-point has the symmetry $\Gamma_{25'}$ and is 3-fold degenerate. The energy spectrum near the Γ-point is determined by a generalization of the Luttinger Hamiltonian in the spherical approximation.[32] The three following types of the hole wave function can be distinguished:

$$\Psi_{FM}^{hm}(\boldsymbol{r}) = R_F^{F-1}(r)\, \mathsf{Y}_{FM}^{F-1}(\hat{\boldsymbol{r}}) + R_F^{F+1}(r)\, \mathsf{Y}_{FM}^{F+1}(\hat{\boldsymbol{r}}), \quad (1)$$

$$\Psi_{FM}^{hh}(\boldsymbol{r}) = R_F^{F}(r)\, \mathsf{Y}_{FM}^{F}(\hat{\boldsymbol{r}}), \quad (2)$$

$$\Psi_{M}^{hl}(\boldsymbol{r}) = R_0^{1}(r)\, \mathsf{Y}_{0M}^{1}(\hat{\boldsymbol{r}}). \quad (3)$$

Here $\hat{\boldsymbol{r}} = \boldsymbol{r}/r$, F is the hole total angular momentum, M is its projection onto the z-axis, Y_{FM}^{L} ($L = F \pm 1, F$) are the vector spherical harmonics defined as in Ref. 45 with vector components corresponding to the Bloch functions with the appropriate transformational properties (see Appendix 1), and $R_F^{L}(r)$ are the radial wave functions formed by spherical Bessel functions with coefficients determined by the boundary conditions. The boundary conditions are derived assuming the flux continuity at the NC boundary and an isotropic band for the corresponding hole states in SiO$_2$ characterized by the heavy mass $m_{\text{out}} = 10 m_0$, where m_0 is the free electron mass, and the energy barrier $U_{\text{h}} = 4.3$ eV. More details are given in Ref. 31. The calculated dependence of the
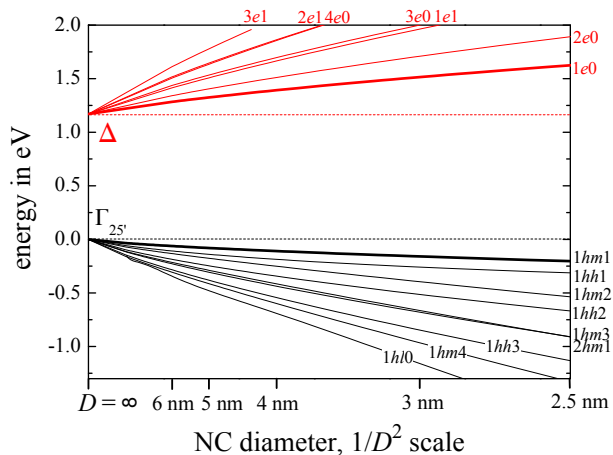
FIG. 1. (Color online) Calculated levels of holes and Δ-electrons in a spherical Si NC surrounded by SiO$_2$ as functions of the NC diameter D.

quantized energy levels of the holes in Si/SiO$_2$ NCs on the NC size is shown in Fig. 1.

The hole states are characterized by the total angular momentum F and by the parity. The states with the parity $(-1)^F$ are the heavy hole (hh) states while the states with the parity $(-1)^{F+1}$ are contributed by both the light and the heavy hole states (mixed hole states: hm) with the only exception for $F = 0$ when the hole states are only contributed by the light holes (hl). The hole states are described by the main quantum number $n = 1, 2, 3...$ followed by the abbreviation hh, hm or hl and the index denoting the total angular momentum F. For example, the hole state with the lowest energy is of the mixed type, namely $1hm1$.

B. Hamiltonian of the problem

Our aim is to calculate the time of the hole multiphonon nonradiative transition between the initial state 2 and the final state 1. Note that in our model both the states 1 and 2 are degenerate with respect to the total angular momentum projection M. In what follows we will use the notation $|i, M\rangle \equiv |n\sigma F, M\rangle$, where $\sigma = hm, hh, hl$ and $i = 1, 2$, to specify one of the functions (1)–(3) for the initial and final states. The Hamiltonian of the problem can be represented as follows:

$$\mathcal{H} = \mathcal{H}_1 + \mathcal{H}_2 + \mathcal{H}^{(\mathrm{ac})} + \mathcal{H}_0^{(\mathrm{phon})}, \qquad (4)$$

$$\mathcal{H}_i = \sum_{M,M'} c_{i,M}^\dagger c_{i,M'} \Big[\varepsilon_i \delta_{M,M'} \\ + \sum_{\boldsymbol{q},\boldsymbol{\nu}} \langle i, M | \hat{V}_{\mathrm{opt}}(\boldsymbol{u}_{\mathrm{opt}}) | i, M' \rangle \Big], \qquad (5)$$

where $i = 1, 2$; $c_{i,M}$ are the annihilation operators of the holes, and $\hat{V}_{\mathrm{opt}}(\boldsymbol{u}_{\mathrm{opt}})$ is the lattice scattering potential for

holes due to the interaction with optical phonons in Si. The Hamiltonian of the interaction of holes with acoustic phonons is given by

$$\mathcal{H}^{(\mathrm{ac})} = \mathcal{H}_{2\rightarrow1} + \mathcal{H}_{1\rightarrow2}, \qquad (6)$$

where

$$\mathcal{H}_{2\rightarrow1} = \sum_{M,M'} c_{1,M}^\dagger c_{2,M'} \langle 1, M | \hat{V}_{\mathrm{ac}}(\boldsymbol{u}_{\mathrm{ac}}) | 2, M' \rangle, \qquad (7)$$

$\mathcal{H}_{1\rightarrow2} = \mathcal{H}_{2\rightarrow1}^\dagger$, and $\hat{V}_{\mathrm{ac}}(\boldsymbol{u}_{\mathrm{ac}})$ is the lattice scattering potential for holes due to the interaction with acoustic phonons in Si. In what follows we consider transitions from the state 2 to the state 1 promoted by the emission or by the absorption of a single acoustic phonon. In this case the part $H_{1\rightarrow2}$ of the Hamiltonian (6) can actually be neglected in the calculation. The free phonon part of the Hamiltonian (5) reads

$$\mathcal{H}_0^{(\mathrm{phon})} = \hbar\omega_{\mathrm{opt}} \sum_{\boldsymbol{q},\boldsymbol{\nu}} b_{\boldsymbol{q}\boldsymbol{\nu}}^\dagger b_{\boldsymbol{q}\boldsymbol{\nu}} + \hbar \sum_{\boldsymbol{q},\boldsymbol{\nu}} s_\nu q a_{\boldsymbol{q}\boldsymbol{\nu}}^\dagger a_{\boldsymbol{q}\boldsymbol{\nu}}, \qquad (8)$$

where $b_{\boldsymbol{q}\boldsymbol{\nu}}$ and $a_{\boldsymbol{q}\boldsymbol{\nu}}$ are, respectively, the annihilation operators of optical and acoustical phonons with wave vector $\boldsymbol{q}$ and polarization $\boldsymbol{\nu}$; $\hbar\omega_{\mathrm{opt}}$ is the optical phonon energy close to 60 meV for Si. We use the Debye model for the dispersion of longitudinal acoustic (LA) and transversal acoustic (TA) phonons with the sound velocity $s_{\mathrm{LA}} = 9 \times 10^5$ cm/s ($s_{\mathrm{TA}} = 5 \times 10^5$ cm/s) and the Debye energy $\hbar\omega_{\mathrm{LA}}^{\mathrm{D}} = 50$ meV ($\hbar\omega_{\mathrm{TA}}^{\mathrm{D}} = 20$ meV) for LA (TA) phonons.[46] It was shown in Refs. 38,39 that for NCs with diameters $D \gtrsim 4$ nm the interatomic forces remain close to those in the bulk and there are no dramatic changes in the phonon spectrum. Therefore, we consider the electron-phonon interaction using the parameters of bulk Si. A more rigorous treatment of the phonon spectrum is in order for obtaining better quantitative results for small NCs with diameters on the order of 3 nm and smaller, which is out of the scope of the present work.

The lattice scattering potential for holes due to the interaction with the optical phonons in Si reads:[43]

$$\hat{V}_{\mathrm{opt}}(\boldsymbol{u}_{\mathrm{opt}}) = \frac{1}{\sqrt{3}} \frac{d_0}{a_0} \boldsymbol{u}_{\mathrm{opt}} \cdot \hat{\boldsymbol{K}}, \qquad (9)$$

where $a_0 = 5.4$ Å is the lattice constant, d_0 is the interaction constant, and

$$\boldsymbol{u}_{\mathrm{opt}} = \sum_{\boldsymbol{q},\boldsymbol{\nu}} \sqrt{\frac{\hbar}{2\rho_0\omega_{\mathrm{opt}}V}} \left(b_{\boldsymbol{q}\boldsymbol{\nu}}^\dagger \boldsymbol{\nu}_{\boldsymbol{q}}^* e^{-i\boldsymbol{q}\boldsymbol{r}} + b_{\boldsymbol{q}\boldsymbol{\nu}} \boldsymbol{\nu}_{\boldsymbol{q}} e^{i\boldsymbol{q}\boldsymbol{r}} \right) \quad (10)$$

is the continuous field of the sublattice displacement induced by optical phonons, being equal to the half of the relative atomic displacement of the two sublattices. Here V is the normalization volume and $\rho_0 = 2.3$ g/cm^3 is the density of silicon. $\hat{K}_x$ component of $\hat{\boldsymbol{K}}$ is given by

$$\hat{K}_x = \hat{J}_y\hat{J}_z + \hat{J}_z\hat{J}_y, \qquad (11)$$

while $\hat{K}_y$ and $\hat{K}_z$ are given by the cyclic permutations. As the spin-orbit interaction is neglected, the angular momentum matrices $\hat{J}_x$, $\hat{J}_y$, and $\hat{J}_z$ correspond to $J=1$, and we take $d_0 = 70$ eV.[14,47,48] Special care has been given to the choice of the notations and parameters[14] which resulted in slightly different notations as compared to some of our previous works.[23,31]

The lattice scattering potential for holes due to the interaction with acoustic phonons is given by

$$\hat{V}_{\rm ac}(\boldsymbol{u}_{\rm ac}) = \left(a - \frac{2}{3}b\right) \sum_{\alpha=x,y,z} \varepsilon_{\alpha\alpha} + b \sum_{\alpha=x,y,z} \varepsilon_{\alpha\alpha} \hat{J}_\alpha^2 \\ + b(\varepsilon_{xy}\hat{K}_z + \varepsilon_{yz}\hat{K}_x + \varepsilon_{zx}\hat{K}_y), \quad (12)$$

where a and b are the constants of the deformation potential. For Si it was calculated that $a = -10$ eV and $b = 3$ eV.[48] The deformation tensor components $\varepsilon_{\alpha\beta}$ are given by

$$\varepsilon_{\alpha\beta} = \frac{1}{2}\left(\frac{\partial u_\alpha}{\partial x_\beta} + \frac{\partial u_\beta}{\partial x_\alpha}\right), \quad (13)$$

and the atomic displacement field induced by acoustic phonons equals to

$$\boldsymbol{u}_{\rm ac} = \sum_{\boldsymbol{q},\nu} \sqrt{\frac{\hbar}{2\rho_0 s_\nu qV}}(a_{\boldsymbol{q}\nu}^\dagger \boldsymbol{\nu}_{\boldsymbol{q}}^* e^{-i\boldsymbol{q}\boldsymbol{r}} + a_{\boldsymbol{q}\nu}\boldsymbol{\nu}_{\boldsymbol{q}} e^{i\boldsymbol{q}\boldsymbol{r}}). \quad (14)$$

The polarization vectors $\boldsymbol{\nu}_{\boldsymbol{q}}$ in Eqs. (10) and (14) are orthonormalized and can be chosen to be either purely real or purely imaginary.

The Hamiltonian (4) describes the multiphonon relaxation promoted by the emission or the absorption of a single acoustic phonon.[44] The operator given by Eq. (7) supplies a matrix element between the final and initial electronic states necessary to trigger the multiphonon transition. This operator will be treated in the lowest order of the perturbation theory. The multiphonon part of the total Hamiltonian determined by Eq. (5) accounts for the energy difference between the levels ε_2 and ε_1 and is responsible for the transition efficiency. In Sec. II C we will show that this efficiency can be described by the Huang-Rhys factor.

The operators $\mathcal{H}_1$ and $\mathcal{H}_2$ can be rewritten as

$$\mathcal{H}_i = \varepsilon_i \sum_M c_{i,M}^\dagger c_{i,M} \\ + \left(\sum_{M,M'} c_{i,M}^\dagger c_{i,M'} \sum_{\boldsymbol{q}\nu} V_{i,\boldsymbol{q}\nu}^{MM'} b_{\boldsymbol{q}\nu} + h.c.\right), \quad (15)$$

with

$$V_{i,\boldsymbol{q}\nu}^{MM'} = \frac{d_0}{a_0}\sqrt{\frac{\hbar}{6\rho_0\omega_{\rm opt}V}}\langle i, M|e^{i\boldsymbol{q}\boldsymbol{r}}\boldsymbol{\nu}_{\boldsymbol{q}}\cdot\hat{\boldsymbol{K}}|i, M'\rangle, \quad (16)$$

and $\mathcal{H}_{2\rightarrow 1}$ takes the form

$$\mathcal{H}_{2\rightarrow 1} = \sum_{M,M'}\sum_{\boldsymbol{q}\nu} c_{1,M}^\dagger c_{2,M'}\left[V_{12,\boldsymbol{q}\nu}^{MM'} a_{\boldsymbol{q}\nu} + (V_{21,\boldsymbol{q}\nu}^{M'M})^* a_{\boldsymbol{q}\nu}^\dagger\right], \quad (17)$$

where

$$V_{ii',\boldsymbol{q}\nu}^{MM'} = \sqrt{\frac{\hbar}{2\rho_0 s_\nu qV}}\langle i, M|\hat{V}_{\rm ac}(\boldsymbol{\nu}_{\boldsymbol{q}}e^{i\boldsymbol{q}\boldsymbol{r}})|i', M'\rangle. \quad (18)$$

C. Reduction of the problem to the Huang-Rhys model

The calculation of the multiphonon transition rate within the present model is greatly complicated by the degeneracy of the initial and final states with respect to the hole total angular momentum. As the electron-phonon interaction lifts this degeneracy, the exact solution of the problem should proceed, at first, by diagonalizing the Hamiltonians (5) for each given phonon mode $(\boldsymbol{q},\nu)$ and a proper summation over the phonon modes afterwards. Instead, we choose to simplify the problem by reducing it to the well-known Huang-Rhys model[19,41,42] allowing for an analytical solution in a closed form. To that end we will replace each multiplet $\{|i, M\rangle; \; M = -F, ..., F\}$ by a single state $|i\rangle$. Then the operators $\mathcal{H}_i$ take the form

$$\mathcal{H}_i = c_i^\dagger c_i\left[\varepsilon_i + \left(\sum_{\boldsymbol{q},\nu} V_{i,\boldsymbol{q}\nu}b_{\boldsymbol{q}\nu} + h.c.\right)\right], \quad (19)$$

where we have introduced the annihilation operators c_i of the states i and the effective matrix elements V_i, independent of the angular momentum projection. The operator $\mathcal{H}_{2\rightarrow 1}$ reduces to

$$\mathcal{H}_{2\rightarrow 1} = \sum_{\boldsymbol{q},\nu} c_1^\dagger c_2[V_{12,\boldsymbol{q}\nu}a_{\boldsymbol{q}\nu} + V_{21,\boldsymbol{q}\nu}^* a_{\boldsymbol{q}\nu}^\dagger]. \quad (20)$$

A justification of this approximation will be discussed in Sec. II D and Appendix 3.

It is useful to introduce the canonical transformation

$$\mathcal{U}(\alpha) = \exp\left[c^\dagger c(\alpha b^\dagger - \alpha^* b)\right]$$

acting on the fermionic c, $c^\dagger$ and bosonic operators b, $b^\dagger$ as follows:

$$\mathcal{U}b\mathcal{U}^{-1} = b - \alpha c^\dagger c, \quad \mathcal{U}b^\dagger\mathcal{U}^{-1} = b^\dagger - \alpha^* c^\dagger c, \\ \mathcal{U}c\mathcal{U}^{-1} = \exp[-(\alpha b^\dagger - \alpha^* b)]c, \\ \mathcal{U}c^\dagger\mathcal{U}^{-1} = \exp[(\alpha b^\dagger - \alpha^* b)]c^\dagger.$$

In particular, the transformation

$$\mathcal{U} = \exp\left\{\sum_{\boldsymbol{q},\nu}\frac{1}{\hbar\omega_{\rm opt}}(c_2^\dagger c_2 + c_1^\dagger c_1) \\ \times\left[V_{2,\boldsymbol{q}\nu}^* b_{\boldsymbol{q}\nu}^\dagger - V_{2,\boldsymbol{q}\nu} b_{\boldsymbol{q}\nu}\right]\right\} \quad (21)$$

changes $\mathcal{H}_2 + \mathcal{H}_1$ to

$$c_2^\dagger c_2 \left[\varepsilon_2 - \sum_{\boldsymbol{q},\boldsymbol{\nu}} \frac{|V_{2,\boldsymbol{q}\boldsymbol{\nu}}|^2}{\hbar\omega_{\mathrm{opt}}}\right]$$
$$+ c_1^\dagger c_1 \left[\varepsilon_1 + \sum_{\boldsymbol{q},\boldsymbol{\nu}} \frac{|V_{2,\boldsymbol{q}\boldsymbol{\nu}}|^2 - 2\,\mathrm{Re}\left[V_{2,\boldsymbol{q}\boldsymbol{\nu}} V_{1,\boldsymbol{q}\boldsymbol{\nu}}^*\right]}{\hbar\omega_{\mathrm{opt}}}\right] \quad (22)$$
$$+ \left\{c_1^\dagger c_1 \sum_{\boldsymbol{q},\boldsymbol{\nu}} [V_{1,\boldsymbol{q}\boldsymbol{\nu}} - V_{2,\boldsymbol{q}\boldsymbol{\nu}}] b_{\boldsymbol{q}\boldsymbol{\nu}} + h.c.\right\}$$

and does not change the form of the Hamiltonian $\mathcal{H}^{(\mathrm{ac})} + \mathcal{H}_0^{(\mathrm{phon})}$. As a result of this transformation, the diagonal electron-phonon interaction is present only for the lower state and the Hamiltonian $\mathcal{H}_2 + \mathcal{H}_1$ is similar to that considered in Ref. 19 after the substitutions

$$\varepsilon_2 \to \varepsilon_2 - \sum_{\boldsymbol{q},\boldsymbol{\nu}} \frac{|V_{2,\boldsymbol{q}\boldsymbol{\nu}}|^2}{\hbar\omega_{\mathrm{opt}}},$$
$$\varepsilon_1 \to \varepsilon_1 + \sum_{\boldsymbol{q},\boldsymbol{\nu}} \frac{|V_{2,\boldsymbol{q}\boldsymbol{\nu}}|^2 - 2\,\mathrm{Re}\left[V_{2,\boldsymbol{q}\boldsymbol{\nu}} V_{1,\boldsymbol{q}\boldsymbol{\nu}}^*\right]}{\hbar\omega_{\mathrm{opt}}}$$

are made. Thus, the rate W_p of a transition assisted by the emission of p optical phonons and promoted by a single acoustic phonon is given by[19,32,41,42]

$$W_p(T) = \frac{1}{\tau_{\mathrm{ac}}(T)} J_p(T,S). \quad (23)$$

Here S is the Huang-Rhys factor, T is the temperature, $\tau_{\mathrm{ac}}(T)$ is the time determined by the acoustic phonon emission,

$$J_p(T,S) = \exp\left[-2S\left(N_{\hbar\omega_{\mathrm{opt}}} + \frac{1}{2}\right)\right] \exp\left(\frac{p}{2}\frac{\hbar\omega_{\mathrm{opt}}}{k_{\mathrm{B}}T}\right)$$
$$\times I_p\left(2S\sqrt{N_{\hbar\omega_{\mathrm{opt}}}(N_{\hbar\omega_{\mathrm{opt}}} + 1)}\right), \quad (24)$$

where

$$N_E = \frac{1}{\exp\frac{E}{k_{\mathrm{B}}T} - 1} \quad (25)$$

is the Bose-Einstein factor at the optical phonon energy E, with k_{B} being the Boltzmann constant, and I_p is the modified Bessel function. For $S \ll 1$ and $k_{\mathrm{B}}T \ll \hbar\omega_{\mathrm{opt}}$ the value of $J_p(T,S)$ can be well approximated by

$$J_p(T,S) \approx \frac{\left[S(N_{\hbar\omega_{\mathrm{opt}}} + 1)\right]^p}{p!}, \quad (26)$$

which has only a very weak temperature dependence as, under these conditions, $N_{\hbar\omega_{\mathrm{opt}}} \ll 1$. One can see that in this case the transition rate strongly depends on S while its temperature dependence is mainly determined by $\tau_{\mathrm{ac}}(T)$. The Huang-Rhys factor can be expressed as

$$S = \frac{1}{(\hbar\omega_{\mathrm{opt}})^2} \sum_{\boldsymbol{q},\boldsymbol{\nu}} |V_{2,\boldsymbol{q}\boldsymbol{\nu}} - V_{1,\boldsymbol{q}\boldsymbol{\nu}}|^2. \quad (27)$$

The number of emitted optical phonons p is given by the integral part of

$$\frac{\varepsilon_2 - \varepsilon_1}{\hbar\omega_{\mathrm{opt}}} + (\delta_{\mathrm{p},2} - \delta_{\mathrm{p},1}) \quad (28)$$

where the total polaron correction $\delta_{\mathrm{p}} = \delta_{\mathrm{p},2} - \delta_{\mathrm{p},1}$ is determined by the difference of the polaron corrections corresponding to the single levels involved in the transition:

$$\delta_{\mathrm{p},i} = -\frac{1}{(\hbar\omega_{\mathrm{opt}})^2} \sum_{\boldsymbol{q},\boldsymbol{\nu}} |V_{i,\boldsymbol{q}\boldsymbol{\nu}}|^2. \quad (29)$$

The reciprocal time of the single acoustic phonon emission (absorption) process is given by

$$\frac{1}{\tau_{\mathrm{ac}}(T)} = \frac{2\pi}{\hbar} \sum_{\boldsymbol{q},\boldsymbol{\nu}} |V_{21,\boldsymbol{q}\boldsymbol{\nu}}|^2 \Big[(N_{\hbar s_\nu q} + 1)\,\delta(\Delta\varepsilon - \hbar s_\nu q)$$
$$+ N_{\hbar s_\nu q}\,\delta(\Delta\varepsilon + \hbar s_\nu q)\Big], \quad (30)$$

where the energy excess (or deficit) $\Delta\varepsilon$ is given by

$$\Delta\varepsilon = \varepsilon_2 - \varepsilon_1 - (p - \delta_p)\hbar\omega_{\mathrm{opt}}. \quad (31)$$

The key feature of the Huang-Rhys model is the factorized form of the transition rate with the acoustic-phonon transition rate and the multiphonon factor entering as the multipliers. Thus, we can calculate the two factors independently.

D. Multiphonon factor

It is convenient to formally introduce the wave functions $\Psi_{1,2}$ by writing the matrix elements $V_{1,\boldsymbol{q}\boldsymbol{\nu}}$ and $V_{2,\boldsymbol{q}\boldsymbol{\nu}}$ in the form

$$V_{i,\boldsymbol{q}\boldsymbol{\nu}} = \frac{d_0}{a_0}\sqrt{\frac{\hbar}{6\rho_0\omega_{\mathrm{opt}}V}} \langle i|e^{\mathrm{i}\boldsymbol{q}\boldsymbol{r}}\boldsymbol{\nu}_{\boldsymbol{q}}\cdot\hat{\boldsymbol{K}}|i\rangle, \quad (32)$$

analogous to Eq. (16). As shown in Appendix 1, this enables one to express the Huang-Rhys factor (27) in the form

$$S = \sigma_{\mathrm{h}} R^3 \int d\boldsymbol{r} \sum_{\alpha=x,y,z} |\Psi_1^\dagger \mathsf{K}_\alpha \Psi_1 - \Psi_2^\dagger \mathsf{K}_\alpha \Psi_2|^2, \quad (33)$$

where R is the NC radius and we have introduced the dimensionless factor

$$\sigma_{\mathrm{h}} = \frac{d_0^2}{6\hbar\omega_{\mathrm{opt}}^3 a_0^2 \rho_0 R^3}. \quad (34)$$

Similarly, the polaron corrections, given by Eq. (29), can be written as

$$\delta_{\mathrm{p},i} = -\sigma_{\mathrm{h}} R^3 \int d\boldsymbol{r} \sum_{\alpha=x,y,z} |\Psi_i^\dagger \mathsf{K}_\alpha \Psi_i|^2. \quad (35)$$
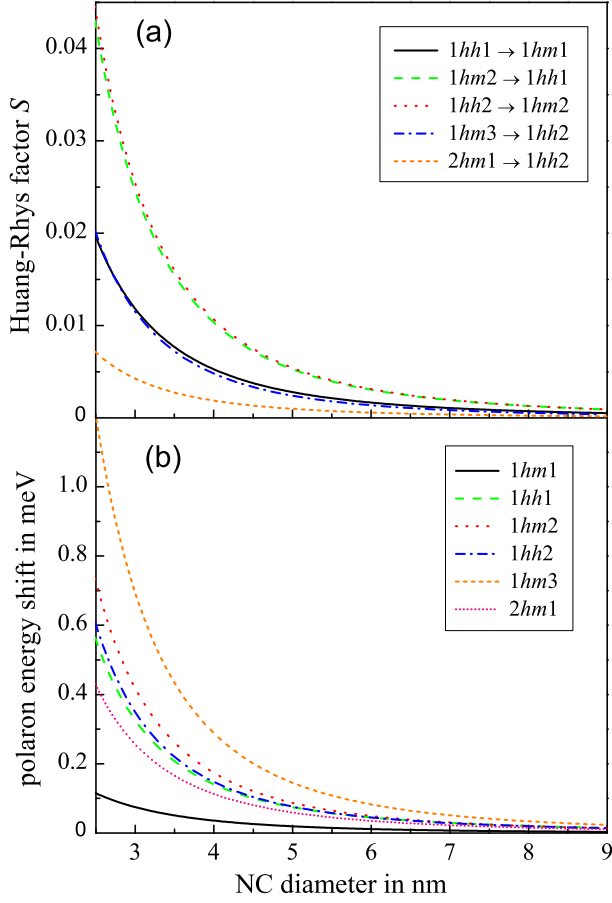
FIG. 2. (Color online) (a) Dependence of the hole Huang-Rhys factor S on the NC diameter for the transitions between the six lowest hole levels. (b) Dependence of the polaron energy shifts $-\delta_{\mathrm{p},i}\hbar\omega_{\mathrm{opt}}$ determined by Eq. (37) on the NC diameter for the transitions between the six lowest hole levels.

We have already mentioned that an exact calculation of the relaxation time would require the diagonalization of the operators (5). This would involve the evaluation of quadratic forms such as $\Psi_i^\dagger \mathsf{K}_\alpha \Psi_i$ using the correct basis of the wave functions in the zeroth-order approximation. However, the quadratic form $\sum_M \Psi_{F,M}^{\sigma,\dagger} \mathsf{K}_\alpha \Psi_{F,M}^\sigma$ does not depend on the choice of the basis. Therefore, as an approximation, we replace the matrix elements $\Psi_i^\dagger \mathsf{K}_\alpha \Psi_i$ by their values averaged over M:

$$S = \sigma_{\mathrm{h}} R^3 \int \mathrm{d}\boldsymbol{r} \sum_{\alpha=x,y,z} \Big| \frac{1}{2F_1+1} \sum_{M_1} \Psi_{F_1,M_1}^{\sigma_1,\dagger} \mathsf{K}_\alpha \Psi_{F_1,M_1}^{\sigma_1} - \frac{1}{2F_2+1} \sum_{M_2} \Psi_{F_2,M_2}^{\sigma_2,\dagger} \mathsf{K}_\alpha \Psi_{F_2,M_2}^{\sigma_2} \Big|^2. \tag{36}$$

Possible derivation procedures justifying this type of averaging are discussed in Appendix 3.

Dependence of the hole Huang-Rhys factor S given by Eq. (36) on the NC diameter D for the transitions between the six lowest hole levels is shown in Fig. 2a. One

can see that for all the transitions the value of the Huang-Rhys factor increases as the NC diameter decreases, approximately as $1/D^3$, but remains below 0.05 for all considered transitions and NC sizes. Therefore, Eq. (26) provides a good approximation of the multiphonon factor which is suitable for the estimation of its contribution to the total transition rate. Nevertheless, in our numerical calculations we use the full form of Eq. (24).

The polaron corrections (35) for each level have now the form

$$\delta_{\mathrm{p},i} = -\sigma_{\mathrm{h}} R^3 \int \mathrm{d}\boldsymbol{r} \sum_{\alpha=x,y,z} \Big| \frac{1}{2F_i+1} \sum_{M_i} \Psi_{F_i,M_i}^{\sigma_i,\dagger} \mathsf{K}_\alpha \Psi_{F_i,M_i}^{\sigma_i} \Big|^2. \tag{37}$$

One can see from Fig. 2b that the values of $\delta_{\mathrm{p},i}$ are small. This guarantees that the splittings of each multiplet $|i,M\rangle$ induced by the hole coupling to optical phonons are also small and our two-level approximation (15) is justified. Since the polaron corrections are significantly smaller than the optical phonon energy, we have neglected them in the numerical calculations of the relaxation times.

E. Acoustic phonon part

The acoustic phonon transition rate $1/\tau_{\mathrm{ac}}$ is given by

$$\frac{1}{\tau_{\mathrm{ac}}} = \frac{1}{F_2+1} \sum_{M_1,M_2} \left(\frac{1}{\tau_{\mathrm{ac}}} \right)_{M_2,M_1}, \tag{38}$$

where the partial rates $(1/\tau_{\mathrm{ac}})_{M_2,M_1}$ describing the transitions $|2,M_2\rangle \to |1,M_1\rangle$ and given by Eq. (30) after the substitution $V_{21,\boldsymbol{q}\nu} \to V_{21,\boldsymbol{q}\nu}^{M_2 M_1}$ are averaged over the initial and summed over the final states.

After the integration over q in Eq. (30) we obtain

$$\left(\frac{1}{\tau_{\mathrm{ac}}} \right)_{M_2,M_1} = \int \frac{\mathrm{d}\Omega_{\boldsymbol{q}}}{4\pi} \sum_\nu \frac{|\Delta\varepsilon|^3 \left[N_{\hbar\omega} + 1/2 + \mathrm{sgn}(\Delta\varepsilon)/2 \right]}{2\pi\hbar^4 \rho_0 s_\nu^5}$$
$$\times \Theta(\hbar\omega_\nu^{\mathrm{D}} - |\Delta\varepsilon|)$$
$$\times \Big| \int \mathrm{d}\boldsymbol{r} \Psi_{F_2,M_2}^{\sigma_2,\dagger}(\boldsymbol{r}) \mathsf{H}_\nu^{\hat{\boldsymbol{q}}} e^{\mathrm{i}\boldsymbol{qr}} \Psi_{F_1,M_1}^{\sigma_1}(\boldsymbol{r}) \Big|^2, \tag{39}$$

where $\mathrm{sgn}(\Delta\varepsilon) = \pm 1$ corresponds to the phonon emission (absorption), and the absolute value of the vector $\boldsymbol{q}$ equals to $|\Delta\varepsilon|/s_\nu$. The function $\Theta(x)$ in Eq. (39) is the Heavyside function, $\hat{\boldsymbol{q}} = \boldsymbol{q}/q$, and the matrices $\mathsf{H}_\nu^{\hat{\boldsymbol{q}}}$ are given in Appendix 2. The plane wave expansion[45]

$$e^{\mathrm{i}\boldsymbol{qr}} = 4\pi \sum_{lm} \mathrm{i}^l Y_{lm}^*(\hat{\boldsymbol{q}}) Y_{lm}(\hat{\boldsymbol{r}}) j_l(qr) \tag{40}$$

allows one to integrate over $\mathrm{d}\Omega_{\boldsymbol{q}}$ and to rewrite Eq. (39)

as

$$\left(\frac{1}{\tau_{\mathrm{ac}}}\right)_{M_2,M_1} = \sum_{\nu=L,T_1,T_2} \frac{|\omega|^3 \left[N_{\hbar\omega} + 1/2 + \mathrm{sgn}(\Delta\varepsilon)/2\right]}{2\pi\hbar\rho_0 s_\nu^5}$$
$$\times \Theta(\omega_\nu^{\mathrm{D}} - |\omega|) \qquad (41)$$
$$\times \sum_{lml'm'} \sum_{\gamma\delta\gamma'\delta'} \Omega_{\gamma\delta\gamma'\delta'}^{lml'm'}(\nu) J_{lm}^{\gamma\delta*} J_{l'm'}^{\gamma'\delta'},$$

where $\gamma, \delta, \gamma', \delta' = -1, 0, 1$. Here we introduced $\omega = \Delta\varepsilon/\hbar$,

$$J_{lm}^{\gamma\delta} = \int d\boldsymbol{r} \, [\Psi_{2,M_2}^{\sigma_2}]^{\gamma*}(\boldsymbol{r}) j_l(qr) Y_{lm}(\hat{\boldsymbol{r}}) [\Psi_{1,M_1}^{\sigma_1}]^{\delta}(\boldsymbol{r}), \quad (42)$$

and

$$\Omega_{\gamma\delta\gamma'\delta'}^{lml'm'}(\nu) = 4\pi \mathrm{i}^{l'-l} \int d\Omega_{\boldsymbol{q}} \, Y_{lm}(\hat{\boldsymbol{q}}) Y_{l'm'}^*(\hat{\boldsymbol{q}})$$
$$\times [\mathsf{H}_\nu^{\hat{\boldsymbol{q}}}]_{\gamma\delta}^* [\mathsf{H}_\nu^{\hat{\boldsymbol{q}}}]_{\gamma'\delta'}. \qquad (43)$$

The calculated rate of the acoustic phonon emission (absorption) $1/\tau_{\mathrm{ac}}$ is shown in Fig. 3 as a function of the phonon energy. One can see that the rate varies with $\Delta\varepsilon$ over several orders of magnitude. The rate has discontinuities at $\Delta\varepsilon = \pm 20$ eV corresponding to the maximum TA phonon energy, and vanishes at $|\Delta\varepsilon| > 50$ eV, where the LA phonon dispersion saturates. Fig. 3a shows the rate of the transition $1hh1 \rightarrow 1hm1$ at room temperature. Various curves correspond to different NC diameters D. One can see that, for the processes describing the phonon emission, the maximum of the rate decreases with the NC size and shifts towards lower energies. Fig. 3b shows the rate of the transition between the same hole states in a NC of the diameter $D = 4$ nm but for various temperatures. The dependence on the temperature appears solely due to the temperature-dependent equilibrium phonon population, $N_{\hbar\omega}$, leading to a considerable asymmetry between the processes involving the phonon emission and the absorption below $T = 77$ K. In Fig. 3c we compare the emission rate for the transitions between the six lowest levels of the holes.

F. Transitions with emission of multiple acoustic phonons

We have considered the relaxation processes due to the emission of multiple acoustic phonons. Calculations based on Refs. 23, 32, and 49 show that the main contribution to the transition rate comes from the acoustic phonons with energies being about 20 meV. For such phonons $\left|\langle 1|e^{i\boldsymbol{qr}}|1\rangle - \langle 2|e^{i\boldsymbol{qr}}|2\rangle\right|$ is at maximum. The multiphonon processes can be described by a Huang-Rhys factor, which is of the same order as for the optical phonons. However, the emission of several acoustic phonons instead of one optical phonon is much less efficient and may be neglected for both electrons and holes. In the case of small energy spacings between the considered levels, i.e. less than the half of the maximal acoustic

phonon energy, processes involving two acoustic phonons are less effective than the emission of a single acoustic phonon, as it can be expected.[22]

G. Transitions without acoustic phonon emission or absorption

Next we consider relaxation processes where only optical phonons are emitted. Such transitions become possible if one goes beyond the Condon approximation and takes into account the non-adiabaticity of the electron-phonon system.[19,32,44] To that end we include the matrix elements of the hole coupling with optical phonons taken between the hole states 1 and 2 into the Hamiltonian (4). Using the result of Ref. 19 in the limit $S \ll 1$, $k_{\mathrm{B}}T \ll 1$ and generalizing it to include the degeneracy of the hole states, we obtain the average value of the transition probability:

$$\overline{W}_p = 2\pi\omega_{\mathrm{opt}}(N_{\hbar\omega_{\mathrm{opt}}} + 1)^p \frac{S^{p-1}}{(p-1)!}\left(Z + Y\frac{p-1}{S}\right), \quad (44)$$

where $p \geq 1$ is the number of emitted optical phonons and the averaging is produced over the transition energy in the range of the optical phonon energy $\hbar\omega_{\mathrm{opt}}$. Here we defined

$$Z = \frac{1}{2F_2 + 1}\sum_{M_1,M_2} Z_{M_1,M_2}, \qquad (45)$$

$$Y = \frac{1}{2F_2 + 1}\sum_{M_1,M_2} Y_{M_1,M_2}, \qquad (46)$$

where

$$Z_{M_1,M_2} = \sigma_{\mathrm{h}} R^3 \int d\boldsymbol{r} \sum_{\alpha=x,y,z} \left|\Psi_{F_1,M_1}^{\sigma_1,\dagger} \mathsf{K}_\alpha \Psi_{F_2,M_2}^{\sigma_2}\right|^2, \quad (47)$$

$$Y_{M_1,M_2} = \sigma_{\mathrm{h}}^2 R^6 \int d\boldsymbol{r} \sum_{\alpha=x,y,z} \left|\left(\Psi_{F_1,M_1}^{\sigma_1,\dagger} \mathsf{K}_\alpha \Psi_{F_2,M_2}^{\sigma_2}\right)\right.$$
$$\left.\times \left(\Psi_{F_1,M_1}^{\sigma_1,\dagger} \mathsf{K}_\alpha \Psi_{F_1,M_1}^{\sigma_1} - \Psi_{F_2,M_2}^{\sigma_2,\dagger} \mathsf{K}_\alpha \Psi_{F_2,M_2}^{\sigma_2}\right)\right|^2. \quad (48)$$

Calculations using Eq. (44) lead to very high average transitions rates: e.g. for the transition $1hh1 \rightarrow 1hm1$ with a single optical phonon emission we get the transition time on the order of 0.1 ps for NCs with diameters close to 5 nm. However, as it was noticed previously,[18] such transitions are effective only if the difference in the level energies is confined to very narrow energy intervals close to the multiple integer of the optical phonon energy at the Γ-point. As in the case of acoustic phonons, the transition matrix element contains an oscillating form factor $\exp(i\boldsymbol{qr})$ [cf. Eq. (16) and Eq. (18)]. This matrix element decays rapidly when q exceeds a value on the
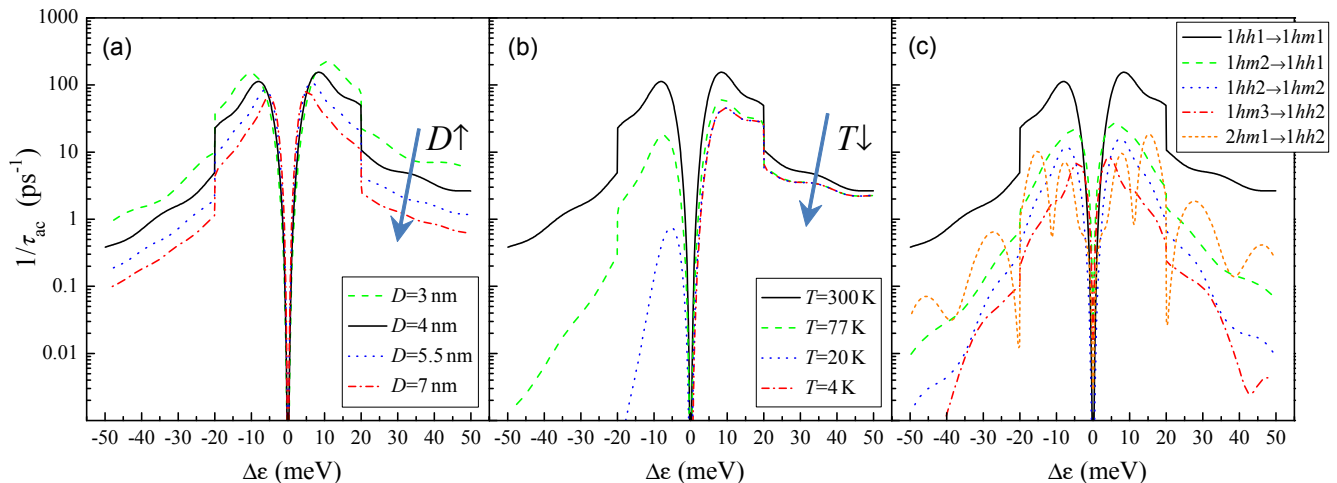
FIG. 3. (Color online) Dependence of the acoustic phonon transition rate $1/\tau_{ac}$ on the energy of the acoustic phonon (a) for the $1hh1 \rightarrow 1hm1$ transition at the temperature $T = 300$ K and different NC diameters D, (b) for the $1hh1 \rightarrow 1hm1$ transition in a NC of $D = 4$ nm at different temperatures T, and (c) for different transitions in a NC of $D = 4$ nm at $T = 300$ K. Positive (negative) acoustic phonon energies correspond to the phonon emission (absorption).

order of π/D that limits the energy intervals where the transition is efficient (see Fig. 3 concerning the acoustic phonons). These intervals are much narrower for optical phonons than for acoustic phonons. This occurs because of the following reasons. First, the energy dispersion of the optical phonons is significantly flatter as compared with the case of the acoustic phonons. As a consequence, for the same value of the wave vector q the deviation of the phonon energy from the phonon energy at the Γ point is much smaller. Secondly, the wave-vector-dependent matrix element of the charge carrier interaction with acoustic phonons is proportional to q^3 whereas it is only q^2 for optical phonons.[50]

In what follows we will neglect phonon-induced relaxation processes involving emission of only optical phonons. However, one should bear in mind that for each pair of neighboring levels such processes can be efficient for a very small part of NCs in a realistic NC ensemble with a certain size dispersion.

H. Total transition rate

The results of the preceding sections have been implemented to calculate the total multiphonon relaxation rate. The size dependencies of the total rates for multiphonon transitions between the six lowest hole levels are summarized in Fig. 4. Fig. 4a shows the interlevel energy intervals in units of the optical phonon energy $\hbar\omega_{opt}$. Fig. 4b sketches the relative energy positions of the valence-band electron levels. Figs. 4c and d give the size dependencies of the total transitions rates at $T = 300$ K and $T = 77$ K, respectively. In Figs. 4a–d the same color code is used to distinguish various transitions.

The multiphonon transition rate given by Eq. (23) vanishes when the energy of the promoting acoustic phonon

$\Delta\varepsilon$ tends to zero. This occurs whenever one of the curves in Fig. 4a (determining the size dependence of the energy corresponding to a given transition) intersects with one of the horizontal grid lines separated by the energy of the optical phonon. This would lead to dips in the size dependence of the corresponding transition rate like the one shown in Fig. 4c, upper panel, by the dotted line. In reality such dips should not be expected because of the small but not vanishing dispersion of the (bulk-like) optical phonon. In order to take this effect into account approximately, we have "cut" the dips for $|\Delta\varepsilon| < 2.5$ meV while calculating the dependencies presented in Figs. 4c and d.

Analyzing the general trend of the dependence of the transition rate with decreasing the NC diameter we see that the rate stays more or less the same on average for the transitions $1hh1 \rightarrow 1hm1$ and $1hh2 \rightarrow 1hm2$ whereas it decreases for transitions $1hm2 \rightarrow 1hh1$, $1hm3 \rightarrow 1hm1$ and $2hm1 \rightarrow 1hm2$. In order to understand this difference in the behavior we notice that the transition energy dependence on the NC diameter is stronger for the last three of these transitions than for the first two (see Fig. 4a). The multiphonon factor decreases rapidly with the number of the required optical phonons p [see Eq. (26)] because of very small Huang-Rhys factors (see Fig. 2). Although in the same time the acoustic phonon transition rate increases with the NC size decrease (see Fig. 3a) for a fixed phonon energy the NC size dependence of the multiphonon factor is stronger. Therefore we observe a strong decay trend in the transition rate by decreasing the NC size for transitions $1hm2 \rightarrow 1hh1$, $1hm3 \rightarrow 1hm1$ and $2hm1 \rightarrow 1hm2$. The situation is different for transitions $1hh1 \rightarrow 1hm1$ and $1hh2 \rightarrow 1hm2$ because the transition energy dependence on the NC diameter is weaker in this case and the number of the required optical phonons p changes only slowly. For
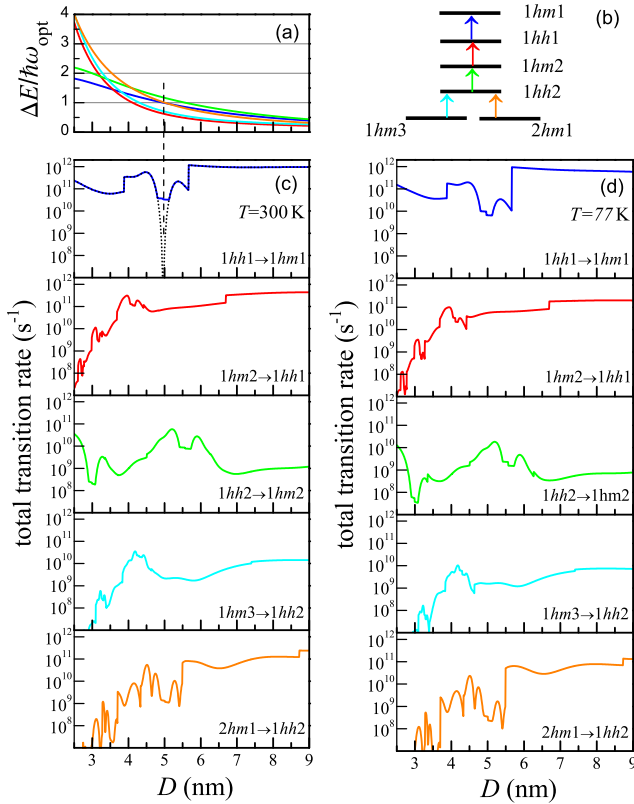
FIG. 4. (Color online) (a) Size dependence of the transition energies between the six lowest hole levels; (b) Scheme of the valence-band electron energy levels; (c) Size dependencies of the multiphonon transition rate for transitions between the six lowest hole levels at $T = 300$ K; (d) same as (c) but for $T = 77$ K. The vertical dashed line in (a) and (c), upper panel, indicates the diameter for which $\Delta E_{1hh1 \to 1hm1} = \hbar\omega_{\text{opt}}$. The solid (dotted) line in (c), upper panel, gives the transition rate calculated with (without) dip exclusion (see text). The dip exclusion has been implemented for all other calculated dependencies of (c) and (d).
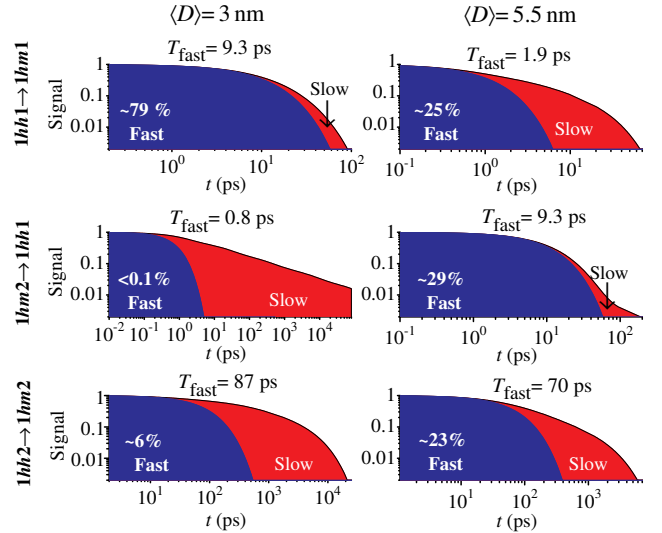

FIG. 5. (Color online) Multiphonon relaxation kinetics for the transitions between the hole levels $1hm1$, $1hh1$, $1hm2$, $1hh2$ (cf. Fig. 4b). The three left and the three right panels correspond to average NC diameters of $\langle D \rangle = 3.0$ nm and $\langle D \rangle = 5.5$ nm, respectively. The upper boundary of the red area for each panel shows the signal decay as a function of time (normalized to the value at $t = 0$). The calculation has been performed for an inhomogeneously broadened ensemble of NCs with the size dispersion $\sigma_{\text{D}} = 0.14\langle D \rangle$. The upper boundary of the blue area represents the exponential curve $\exp(-t/T_{\text{fast}})$, where the relaxation rate $1/T_{\text{fast}}$ is given by Eq. (50). The ratios of the areas under the blue and red curves, representing the relative fraction of the fast component in the signal, are indicated for each panel.

the smallest considered NCs it reaches only $p = 1$ for $1hh1 \to 1hm1$ and $p = 2$ for $1hh2 \to 1hm2$ transitions, respectively. As a consequence, the increase in the acoustic phonon transition rate roughly compensates the decrease in the multiphonon factor.

The effect of temperature on the total transition rate can be estimated comparing Fig. 4c, where $T = 300$ K is used, and Fig. 4d with $T = 77$ K. We see that the rate is smaller in the case of $T = 77$ K by a factor less then 10. This moderate decrease correlates with the temperature dependence of the acoustic phonon transition rate (see Fig. 2). Some of the jumps in the dependencies of the rate on the NC size become larger because contributions with the acoustic phonon absorption ($\Delta\varepsilon < 0$) become much smaller in the case of $T = 77$ K.

A particular feature of the transition rates shown in Figs. 4c and d is their strong dependence on the NC size: The rate may change by several orders of magnitude when the NCs size changes by 10%. It is known

that such dependencies can lead to multi-exponential or stretched-exponential population decays if the size dispersion is taken into account.[51–53] The population decay of a particular selected level within an ensemble of NCs can be found as

$$f(t) = \int P(D) \exp\left[-tW(D)\right] dD \,, \qquad (49)$$

where $f(t)$ is the time-dependent level population normalized to its value at $t = 0$, $P(D)$ stands for the NC size distribution, and $W(D)$ is the size-dependent total transition rate. The corresponding kinetics of the hole level population decay due to the relaxation up to the next neighboring level is illustrated in Fig. 5. We see that only the initial part of the decay is single-exponential with the time T_{fast} determined by

$$\frac{1}{T_{\text{fast}}} = \int P(D)W(D)dD \,. \qquad (50)$$

At a later stage of the relaxation process the kinetics is governed by a much slower decay tail which can be approximately described by the Williams-Watts stretched exponential law.[51,52]

III. INTERVALLEY MULTIPHONON RELAXATION OF CONFINED ELECTRONS

A. Electron size quantization

The conduction-band states in Si NCs originate from the six equivalent Δ-valleys in the conduction band of bulk Si. To calculate their energy levels we employed the approach of Ref. 31. This approach accounts for the strong anisotropy of the conduction band effective mass but neglects the non-parabolicity of the band. This provides a good approximation for moderately excited electrons with energies close to the band minimum. We further neglect the splitting of the electron energy levels arising from the intervalley mixing. The latter is due to the finite size of the NC and depends on the boundary conditions.[28] Our estimations based on the $sp^3d^5s^*$ empirical tight-binding method[11,54] have shown that this orbit-valley splitting is considerably smaller than the interlevel energy gaps for NCs with diameters $D > 3$ nm. However, for smaller NCs it can considerably change the transition energies and affect so the results for the transition rates.

Our approach also takes into account the effect of the electron tunneling into the SiO$_2$ matrix. We assign a finite energy barrier of 3.2 eV[55,56] to Δ-electrons at the Si/SiO$_2$ interface and use the mass $m \approx m_0$ for the electrons in SiO$_2$[57]. This leads to the considerable decrease of the energies of confined electrons, and allows for an exceptionally good agreement with the experimental data on indirect photoluminescence.[31] For very small NCs, the effect of tunneling can be dramatic,[25,26,58] leading to considerable penetration of the carrier density beyond the NC boundary and its localization near the NC boundary. The calculated energy levels of Δ-electrons confined in a spherical Si NC surrounded by SiO$_2$ are shown in Fig. 1. The notation for different electron states is the same as in Ref. 31. The electron states are characterized by the angular quantum number $m = 0, 1, 2, ...$ and the main quantum number $n = 1, 2, 3, ...$ The states have the degeneracy of $12m$, including the spin degeneracy. The four lowest electron states ordered by their energies are labeled as $1e0$, $2e0$, $1e1$, and $3e0$, respectively (see Fig. 1).

B. Relaxation via emission of intervalley optical phonons

The intravalley electron scattering on optical phonons is absent in bulk Si,[43] so the ordinary multiphonon processes,[19] described within the framework of the Huang-Rhys model,[32,41,42] are ruled out for electrons in Si NCs. However, the optical phonons in bulk Si can cause scattering of the electrons between different Δ valleys in the conduction band.[59,60] Such processes play an important role the in energy relaxation in bulk Si.[61-64] In this work we analyze their contribution to the energy relaxation in Si NCs. We consider emission of $p \geq 1$ intervalley optical phonons accompanied by the emission or the absorption of a single intravalley acoustic phonon. The participation of the acoustic phonon in the relaxation process ensures the overall energy conservation.

It was shown in Refs. 38 and 39 that for NCs with sizes 4 nm $< D < 8$ nm the interatomic forces remain close to those in the bulk and there are no dramatic changes in the phonon spectrum. These results enable us to analyze the electron-phonon interaction using the bulk values of the deformation potential. Since the conduction band of bulk Si has six equivalent Δ-valleys, each state of the confined electron has an additional sixfold degeneracy. We restrict ourselves to the so-called g processes responsible for the coupling of the electron states in opposite Δ valleys.[33,61] Three groups of the electron states can be distinguished, as there are three degenerate pairs of opposite Δ valleys. The interaction of the electrons with the g phonons takes place within each group independently. The energy of the g optical phonon in bulk Si is $\hbar\omega_{\mathrm{opt}} = 63$ meV.[65] We use the approximate value of 60 meV. The energy difference between the initial and the final states is not necessarily equal to the integral number of optical phonon energies $\hbar\omega_{\mathrm{opt}}$. Therefore, we also take into account the acoustic phonons; their close-to-linear energy dispersion allows one to fulfill the energy conservation law. We consider the intravalley matrix elements of the electron interaction with the acoustic phonons via the deformation potential. Similar to the case of holes (cf. Sec. II H), we take into account the weak optical phonon energy dispersion[46] when the energy of the promoting acoustic phonon is close to zero.

Let us restrict our consideration by a given pair of valleys. In this case the relaxation problem involves a total of four electron states, which are pairwise valley-degenerate. The pair of initial (final) states is characterized by the envelope function $|i\rangle$ ($|f\rangle$), and the energy E_i (E_f). We will use the notation (n, v) to label the electron states, where the index $n = i, f$ stands for the envelope function and the valley index $v = 1, 2$ specifies the location of the particular Δ extremum in the Brillouin zone, either at the point $\boldsymbol{k}_1 = (k_0, 0, 0)$ or at the opposite point $\boldsymbol{k}_2 = (-k_0, 0, 0)$, where $k_0 = 0.85 \times 2\pi/a_0$.

The processes accompanied by the optical phonon absorption can be safely neglected even at room temperature; $\hbar\omega_{\mathrm{opt}} \gg k_{\mathrm{B}}T$. Thus, we consider the energy relaxation with the emission of p intervalley optical phonons, assisted by single acoustic phonon emission (or absorption). The relaxation process can be thought of consisting of $p + 1$ virtual transitions: p transitions of the type $(i, 1) \leftrightarrow (i, 2)$ or $(f, 1) \leftrightarrow (f, 2)$ (with the emission of the intervalley optical phonon) and one intravalley transition, either $(i, 1) \rightarrow (f, 1)$ or $(i, 2) \rightarrow (f, 2)$, involving an acoustic phonon with energy $\hbar\omega_{\mathrm{ac}} = |E_f - E_i - p\hbar\omega_{\mathrm{opt}}|$. The relaxation process is described by the following Hamilto-

nian:

$$\mathcal{H} = \sum_{v=1,2} (E_i c_{i,v}^\dagger c_{i,v} + E_f c_{f,v}^\dagger c_{f,v}) + \mathcal{H}_0^{(\mathrm{phon})}$$
$$+ \mathcal{H}_i^{(\mathrm{opt})} + \mathcal{H}_f^{(\mathrm{opt})} + \mathcal{H}^{(\mathrm{ac})} . \tag{51}$$

The terms in Eq. (51) are as follows: (i) the free-electron Hamiltonian, where $c_{i,v}$ and $c_{f,v}$ are the corresponding electron annihilation operators, (ii) the free-phonon Hamiltonian $\mathcal{H}_0^{(\mathrm{phon})}$, (iii) the Hamiltonian of the electron interaction with *intervalley* optical phonons $\mathcal{H}_i^{(\mathrm{opt})} + \mathcal{H}_f^{(\mathrm{opt})}$ and (iv) the Hamiltonian of the electron interaction with *intravalley* acoustic phonons $\mathcal{H}^{(\mathrm{ac})} = \mathcal{H}_{i \to f}^{(\mathrm{ac})} + \mathcal{H}_{f \to i}^{(\mathrm{ac})}$, whereby $\mathcal{H}_{f \to i}^{(\mathrm{ac})} = (\mathcal{H}_{i \to f}^{(\mathrm{ac})})^\dagger$ can be neglected due to the problem formulation. The free-phonon Hamiltonian reads

$$\mathcal{H}_0^{(\mathrm{phon})} = \sum_{\boldsymbol{q}} [\hbar\omega_{\mathrm{ac}}(q) a_{\boldsymbol{q}}^\dagger a_{\boldsymbol{q}} + \hbar\omega_{\mathrm{opt}} b_{\boldsymbol{q}}^\dagger b_{\boldsymbol{q}}] , \tag{52}$$

where $a_{\boldsymbol{q}}$ and $b_{\boldsymbol{q}}$ are the annihilation operators of the acoustic and the optical phonons, having the energies $\hbar\omega_{\mathrm{ac}}(q) = \hbar s q$ and $\hbar\omega_{\mathrm{opt}}$, respectively. We take into account only LA phonons and disregard the polarization of intravalley optical phonons. The interaction parts of the total Hamiltonian $\mathcal{H}_{i \to f}^{(\mathrm{ac})}$ and $\mathcal{H}_{i,f}^{(\mathrm{opt})}$ are characterized by the deformation potentials Ξ and D_{iv}, respectively. In particular,

$$\mathcal{H}_{i \to f}^{(\mathrm{ac})} = (c_{f,1}^\dagger c_{i,1} + c_{f,2}^\dagger c_{i,2}) \sum_{\boldsymbol{q}} \left[a_{\boldsymbol{q}} A_{fi,\boldsymbol{q}} + a_{\boldsymbol{q}}^\dagger A_{if,\boldsymbol{q}}^* \right], \tag{53}$$

where the complex coefficients $A_{jj',\boldsymbol{q}}$ are given by

$$A_{jj',\boldsymbol{q}} = -\mathrm{i}\Xi \sqrt{\frac{\hbar q}{\rho_0 s V}} \langle j | e^{\mathrm{i}\boldsymbol{q}\boldsymbol{r}} | j' \rangle \tag{54}$$

with V being the normalization volume. The operators $\mathcal{H}_i^{(\mathrm{opt})}$ and $\mathcal{H}_f^{(\mathrm{opt})}$, contributing to the Hamiltonian of the electron interaction with the intervalley optical phonons,[62] are

$$\mathcal{H}_n^{(\mathrm{opt})} = c_{n,1}^\dagger c_{n,2} H_{n,2 \to 1}^{(\mathrm{opt})} + c_{n,2}^\dagger c_{n,1} H_{n,1 \to 2}^{(\mathrm{opt})} , \tag{55}$$

where

$$H_{n,2 \to 1}^{(\mathrm{opt})} = H_{n,1 \to 2}^{(\mathrm{opt})\dagger} = \sum_{\boldsymbol{q}} \left(B_{n,\boldsymbol{q}} b_{\boldsymbol{q}+\boldsymbol{k}_{2,1}} + B_{n,\boldsymbol{q}}^* b_{\boldsymbol{q}+\boldsymbol{k}_{1,2}}^\dagger \right),$$
$$\tag{56}$$

$$B_{n,\boldsymbol{q}} = D_{\mathrm{iv}} \sqrt{\frac{\hbar}{2\rho_0 \omega_{\mathrm{opt}} V}} \langle n | e^{\mathrm{i}\boldsymbol{q}\boldsymbol{r}} | n \rangle,$$

and the letter $n = i, f$ denotes the initial and final states. In the summation over $\boldsymbol{q}$ we have singled out the wave vectors $\boldsymbol{k}_{2,1} = -\boldsymbol{k}_{1,2} = (2\pi/a_0)(0.3,0,0)$. The optical phonon wave vector approximately equals either $\boldsymbol{k}_{2,1}$ or $\boldsymbol{k}_{1,2}$, since the overlap integrals with the envelope functions $\langle n | e^{\mathrm{i}\boldsymbol{q}\boldsymbol{r}} | n \rangle$ rapidly decay when the value

of q exceeds $1/R \lesssim k_0$. Consequently, we distinguish between the two types of intervalley optical phonons participating in the transition, having approximately opposite wave vectors and characterized by annihilation operators $b_{\boldsymbol{q}}^{(2 \to 1)} \equiv b_{\boldsymbol{q}+\boldsymbol{k}_{2,1}}$ and $b_{\boldsymbol{q}}^{(1 \to 2)} \equiv b_{\boldsymbol{q}+\boldsymbol{k}_{1,2}}$.

Following Ref. [19] we use the quantum tunneling formalism[66] to obtain the transition rate. The electronic wave function is given by

$$\hat{\Psi}(t) = [\hat{v}_1(t) c_{i,1}^\dagger + \hat{v}_2(t) c_{i,2}^\dagger + \hat{w}_1(t) c_{f,1}^\dagger + \hat{w}_2(t) c_{f,2}^\dagger] |0\rangle , \tag{57}$$

where $|0\rangle$ is the electronic vacuum and $\hat{v}_{1,2}(t)$, $\hat{w}_{1,2}(t)$ are the operators acting on the phonon subsystem. The Schrödinger equation for the wave function (57) in the interaction representation with respect to the free-phonon Hamiltonian $\mathcal{H}_0^{(\mathrm{phon})}$ leads to the following system of equations:

$$\mathrm{i}\hbar \frac{d\hat{v}_1}{dt} = E_i \hat{v}_1 + \widetilde{H}_{i,2 \to 1}^{(\mathrm{opt})} \hat{v}_2,$$
$$\mathrm{i}\hbar \frac{d\hat{v}_2}{dt} = E_i \hat{v}_2 + \widetilde{H}_{i,1 \to 2}^{(\mathrm{opt})} \hat{v}_1,$$
$$\mathrm{i}\hbar \frac{d\hat{w}_1}{dt} = E_f \hat{w}_1 + \widetilde{H}_{f,2 \to 1}^{(\mathrm{opt})} \hat{w}_2 + \widetilde{H}_{i \to f}^{(\mathrm{ac})} \hat{v}_1,$$
$$\mathrm{i}\hbar \frac{d\hat{w}_2}{dt} = E_f \hat{w}_2 + \widetilde{H}_{f,1 \to 2}^{(\mathrm{opt})} \hat{w}_1 + \widetilde{H}_{i \to f}^{(\mathrm{ac})} \hat{v}_2 , \tag{58}$$

where

$$\widetilde{H}_{n,2 \to 1}^{(\mathrm{opt})} = \sum_{\boldsymbol{q}} \left(B_{n,\boldsymbol{q}} e^{-\mathrm{i}\omega_{\mathrm{opt}} t} b_{\boldsymbol{q}}^{(2 \to 1)} + B_{n,\boldsymbol{q}}^* e^{\mathrm{i}\omega_{\mathrm{opt}} t} b_{\boldsymbol{q}}^{(1 \to 2)\dagger} \right),$$

$$\widetilde{H}_{n,1 \to 2}^{(\mathrm{opt})} = \sum_{\boldsymbol{q}} \left(B_{n,\boldsymbol{q}}^* e^{-\mathrm{i}\omega_{\mathrm{opt}} t} b_{\boldsymbol{q}}^{(1 \to 2)} + B_{n,\boldsymbol{q}} e^{\mathrm{i}\omega_{\mathrm{opt}} t} b_{\boldsymbol{q}}^{(2 \to 1)\dagger} \right),$$

$$\widetilde{H}_{i \to f}^{(\mathrm{ac})} = \sum_{\boldsymbol{q}} \left(A_{\boldsymbol{q}} e^{-\mathrm{i}\omega_{\mathrm{ac}}(q) t} a_{\boldsymbol{q}} + A_{\boldsymbol{q}}^* e^{\mathrm{i}\omega_{\mathrm{ac}}(q) t} a_{\boldsymbol{q}}^\dagger \right) .$$

We note that for the energy relaxation problem the interaction with acoustic phonons for the initial state can be neglected. Initial conditions for the system (58) are

$$\hat{v}_1(t=0) = 1, \quad \hat{v}_2(t=0) = \hat{w}_{1,2}(t=0) = 0 . \tag{59}$$

The relaxation rate is given by

$$W_p = \lim_{t \to \infty} \frac{1}{t} [\langle\!\langle \hat{w}_1^\dagger(t) \hat{w}_1(t) \rangle\!\rangle + \langle\!\langle \hat{w}_2^\dagger(t) \hat{w}_2(t) \rangle\!\rangle] , \tag{60}$$

where the double angular brackets denote the averaging over the thermal distribution of the phonon states. The presence of the two sets of optical phonons, $b^{(1 \to 2)}$ and $b^{(2 \to 1)}$, distinguished by the sign of the wave vector projection to the intervalley direction, is the specific feature of the many-valley problem. Therefore, the techniques developed for the single-valley problem case[19,32,41,42] cannot be used to solve it. Nevertheless, in the realistic case of a weak interaction, the relaxation rate can be found by means of the perturbation theory. The perturbation scheme involves the iterative procedure

applied to the system (58) with the expansion of the solution in powers of the operators $\widetilde{H}^{(\mathrm{opt})}$ and $\widetilde{H}^{(\mathrm{ac})}$.

Note that, for a given number p of the emitted optical phonons, the valley number of the final state is $j = 1 + p \mod 2$. Therefore, only one of the terms in Eq. (60) is non-zero:

$$W_p = \lim_{t \to \infty} \frac{1}{t} \langle\!\langle \hat{w}_j^\dagger(t) \hat{w}_j(t) \rangle\!\rangle . \tag{61}$$

The quantity w_j is proportional to the matrix elements of the electron-phonon interaction, $w_j \propto A B^p$. Since we consider dispersionless optical phonons, the energy of the promoting acoustic mode is fixed. The factor describing the interaction with the acoustic phonons can then be separated out. Similar to the case of holes, the resulting expression for the transition rate,

$$W_p = \frac{1}{\tau_{\mathrm{ac}}} J_p , \tag{62}$$

can be written as a product of the acoustic phonon-related prefactor $1/\tau_{\mathrm{ac}}$ and the multiphonon factor J_p (see Appendix 4). Equation (62) is also valid for the case of $p = 0$ when no optical phonons are involved. In this case we have $J_0 = 1$. The time τ_{ac} is given by

$$\frac{1}{\tau_{\mathrm{ac}}} = \frac{\Xi^2}{2\pi\hbar} \frac{\omega_{\mathrm{ac}}^3}{\rho_0 s^5} (N_{\hbar\omega_{\mathrm{ac}}} + 1/2 \pm 1/2) \int \frac{d\Omega_{\boldsymbol{q}}}{4\pi} |\langle f| e^{i\boldsymbol{q}\boldsymbol{r}} |i\rangle|^2 . \tag{63}$$

Here Ξ is the deformation potential for acoustic phonons, $s \equiv s_{\mathrm{LA}}$ is the longitudinal sound velocity. The integration in Eq. (63) is performed over the angles of the wave vector $\boldsymbol{q}$ having the absolute value $|\mathbf{q}| = \omega_{\mathrm{ac}}/s$. The energy of the promoting acoustic phonon reads

$$\hbar\omega_{\mathrm{ac}} = |E_f - E_i - p\hbar\omega_{\mathrm{opt}}| . \tag{64}$$

The sign $+(-)$ in Eq. (63) corresponds to the emission (absorption) of an acoustic phonon. The multiphonon factor J_p is given by

$$J_p = \sigma_{\mathrm{e}}^p (N_{\hbar\omega_{\mathrm{opt}}} + 1)^p \tilde{\alpha}_{i \to f}(p) , \tag{65}$$

where the dimensionless factor

$$\sigma_{\mathrm{e}} = \frac{D_{\mathrm{iv}}^2}{2\hbar\rho_0\omega_{\mathrm{opt}}^3 R^3}, \tag{66}$$

describes the strength of the electron interaction with the optical phonons. The value of the dimensionless quantity $\tilde{\alpha}_{i \to f}(p)$ depends on the initial and final states and on the number of the emitted optical phonons p. The corresponding expressions are derived and discussed in Appendix 4. The factor $\sigma_{\mathrm{e}}\tilde{\alpha}_{i \to f}(1)$ in Eq. (65) plays essentially the same role as the Huang-Rhys factor in the single-valley problem.[19] The perturbation theory used to derive Eqs. (62) and (65) is applicable since $\sigma_{\mathrm{e}}\tilde{\alpha}_{i \to f}(1) \ll 1$. As we checked numerically, the transition rate decreases rapidly, namely approximately as $\left[\sigma_{\mathrm{e}}(N_{\hbar\omega_{\mathrm{opt}}} + 1)\tilde{\alpha}_{i \to f}(1)\right]^p / p!$, when the number p of the
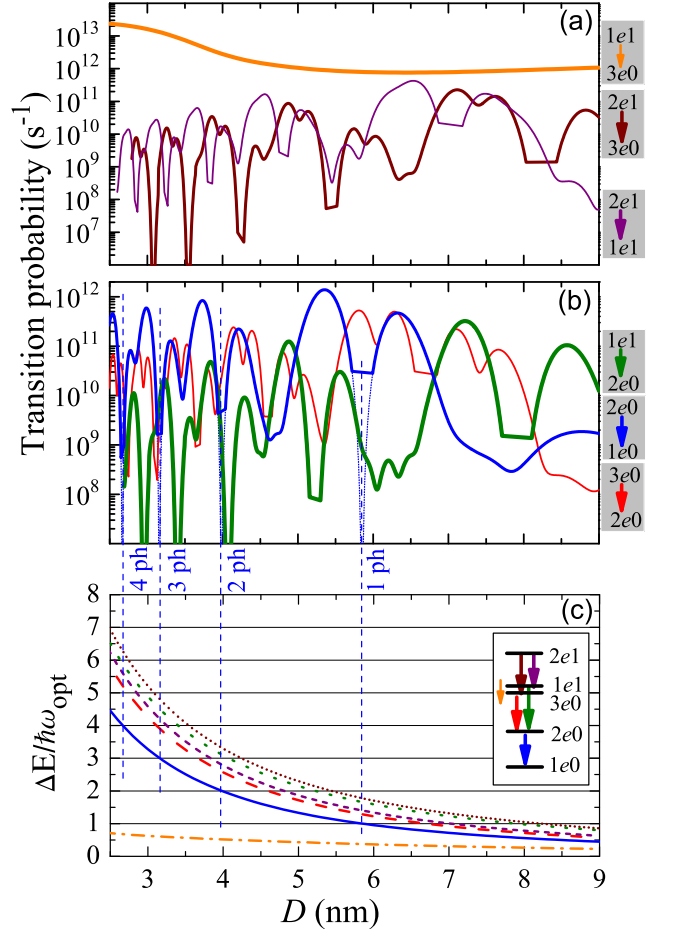

FIG. 6. (Color online) Calculated size dependencies of the total relaxation rate for the following transitions: (a) $1e1 \to 3e0$ (orange line), $2e1 \to 3e0$ (brown line), and $2e1 \to 1e1$ (violet line) and (b) $2e0 \to 1e0$ (blue lines), $3e0 \to 2e0$ (red line), and $1e1 \to 2e0$ (olive line). (c) Size dependence of the transition energies between the lowest electron levels. Inset: Scheme of the conduction-band electron energy levels outlining the color code used to distinguish between various transitions. The vertical dashed lines in (b) and (c) indicate the diameters for which $\Delta E_{2e0 \to 1e0}$ is equal to an integer number of the optical phonon energies, $\hbar\omega_{\mathrm{opt}}$. The solid (dotted) blue line in (b) gives the transition rate calculated with (without) dip exclusion.

emitted optical phonons increases, similarly to Eq. (26). For example, the deviation of this approximation from the result given by Eq. (65) is in the range of $\pm 15\%$ for the transition $1e1 \to 2e0$, depending on the NC size and the number of the emitted phonons.

C. Calculation results

We have calculated the multiphonon factors, the acoustic phonon transition times and the total transition rates between the five lowest electron levels as functions of the NC diameter. The calculations were produced for the

case of room temperature and for the parameter values $\Xi = 10$ eV, $D_{\mathrm{iv}} = 2 \times 10^9$ eV/cm.[33,63] The final results for the total transition rate as a function of the NC diameter are illustrated in Fig. 6. As compared to the case of holes, the typical number of required optical phonons increases more rapidly when decreasing NC size (see Fig. 6c). However, the average transition rates remain relatively high even for small NCs (see Figs. 6a and 6b). This a consequence of a stronger effective electron-phonon interaction leading to larger multiphonon factors as compared to the case of holes.[67]

Similar to the case of holes, we observe that the transition rates as functions of the NC size typically demonstrate a well-pronounced oscillatory behavior, with variations over several orders of magnitude. This leads again to a non-exponential decay of level populations in a NC ensemble.[14] The situation is different when the transition energy is relatively small and the relaxation process involves solely a single acoustic phonon. An example of such process is provided by the $1e1 \rightarrow 3e0$ transition. In this case the electron relaxes rapidly to the lower neighboring level on a time scale of some hundreds of femtoseconds or even faster. The transition time smoothly depends on the NC size.

IV. CONCLUSIONS

We have extended the Huang-Rhys model to the case of the transitions between the degenerate electron and hole levels in Si nanocrystals. Expressions for the multiphonon factors have been found for the electrons using the perturbation theory, which is a good approach as far as we have shown that the electron-phonon interaction is small enough for all considered nanocrystal sizes. These factors contain interference contributions from different possible pathways through the virtual states when multiple intervalley and a single intravalley acoustic phonons are emitted. For holes we have reduced the problem to the Huang-Rhys model introducing average values for the Huang-Rhys factors. We have shown that phonon-induced relaxation of moderately excited electrons and holes in Si nanocrystals occurs typically on the picosecond timescale. The transitions can be even faster if the interlevel energy separation is smaller than

50 meV, which corresponds to the largest possible acoustic phonon energy. The transition times on the order of a nanosecond or even slower are also possible for certain pairs of neighboring levels and nanocrystal sizes. For a given pair of levels the variation of the relaxation rate with the nanocrystal size can amount to several orders of magnitude. Our results suggest that these variations are usually larger for the electron transitions than for the hole transitions. We predict a stretched-exponential behavior of the decay rates in ensembles of Si nanocrystals characterized by a certain size dispersion. The temperature leads to a moderate decrease of the relaxation times due to the increased acoustic phonon populations but does not qualitatively change the their dependencies on the nanocrystal size.

Our results suggest that the carrier relaxation induced by the emission of one or several phonons is a very efficient energy relaxation mechanism for moderately excited carriers in Si nanocrystals. Whereby, in the case of the multiphonon transition, the most effective relaxation pathways are provided by the emission of one or several optical phonons and the emission or the absorption of a single acoustic phonon. Emission of multiple acoustic phonons without optical phonons is relatively ineffective and emission of a single or multiple optical phonons without acoustic phonons can be effective only for a vanishingly small fraction of the nanocrystals. Competing relaxation mechanisms due to radiative intraband transitions[23] and due to transitions induced by the interaction with vibrational modes of the amorphous polar environment[68] lead in most cases to considerably smaller transition rates. One should mention that defects at the NC boundary can introduce competing and even faster relaxation channels. For Si nanocrystals with diameters below 3 nm picosecond and even subpicosecond relaxation lifetimes were predicted under certain conditions.[69] However, these conditions can be very restrictive, especially for moderately excited carriers. The role of the defects in Si NCs surrounded by the SiO_2 matrix needs further detailed investigation.

Appendix 1.

The matrix element in Eq. (32) can be written explicitly as

$$\langle i | e^{\mathrm{i}\boldsymbol{q}\boldsymbol{r}} \boldsymbol{\nu_q} \cdot \hat{\boldsymbol{K}} | i \rangle = \int \mathrm{d}\boldsymbol{r} \, e^{\mathrm{i}\boldsymbol{q}\boldsymbol{r}} \boldsymbol{\nu_q} \cdot \boldsymbol{s}_i(\boldsymbol{r}) \,,$$

where

$$\boldsymbol{s}_i(\boldsymbol{r}) = \Psi_i^\dagger(\boldsymbol{r}) \mathbf{K} \Psi_i(\boldsymbol{r}) \tag{A1.1}$$

and the matrices K_α $(\alpha = x, y, z)$ are defined in Eq. (11). The phonon polarization vectors can be chosen as (in the Cartesian basis)

$$\boldsymbol{\nu}_L = \frac{\boldsymbol{q}}{q}\,,\ \ \boldsymbol{\nu}_{T1} = \frac{1}{\sqrt{q_x^2 + q_y^2}}\,(q_y, -q_x, 0)^T\,,\ \ \boldsymbol{\nu}_{T2} = \frac{1}{q\,\sqrt{q_x^2 + q_y^2}}\,\left[q_x\,q_z, q_y\,q_z, -\left(q_x^2 + q_y^2\right)\right]^T. \tag{A1.2}$$

The orthogonality of the vectors $\boldsymbol{\nu}$ leads to the equation

$$\sum_{\boldsymbol{\nu}} |\boldsymbol{\nu} \cdot \boldsymbol{s}|^2 = s^2$$

and the following identity

$$\frac{1}{V} \sum_{\boldsymbol{q},\boldsymbol{\nu}} \left| \int d\boldsymbol{r}\, e^{i\boldsymbol{q}\boldsymbol{r}} \boldsymbol{\nu} \cdot \boldsymbol{s}_i(\boldsymbol{r}) \right|^2 = \frac{1}{V} \sum_{\boldsymbol{q},\boldsymbol{\nu}} \int d\boldsymbol{r} \int d\boldsymbol{r}'\, [\boldsymbol{\nu} \cdot \boldsymbol{s}_i(\boldsymbol{r})]\,[\boldsymbol{\nu} \cdot \boldsymbol{s}_i(\boldsymbol{r}')]\, e^{i\boldsymbol{q}\,(\boldsymbol{r} - \boldsymbol{r}')}$$

$$= \int d\boldsymbol{r} \sum_{\boldsymbol{\nu}} |\boldsymbol{\nu} \cdot \boldsymbol{s}_i(\boldsymbol{r})|^2 \equiv \int d\boldsymbol{r} \sum_{\alpha = x,y,z} |\Psi_i^\dagger \mathsf{K}_\alpha \Psi_i|^2. \tag{A1.3}$$

Equations (A1.3) allows one to represent Eqs. (27) and (29) as Eqs. (33) and (35), respectively.

To find the values of $\Psi_{F_1,M_1}^{\sigma_1,\dagger} \mathsf{K}_\alpha \Psi_{F_1,M_1}^{\sigma_1}$ in Eqs. (36) and (35) we rewrite the solutions (1)–(3) as

$$\Psi_{FM}^{hm}(\boldsymbol{r}) = \Phi_{FM}^{F-1}(\boldsymbol{r}) + \Phi_{FM}^{F-1}(\boldsymbol{r}), \tag{A1.4}$$

$$\Psi_{FM}^{hh}(\boldsymbol{r}) = \Phi_{FM}^{F}(\boldsymbol{r}), \quad \Psi_{FM}^{hl}(\boldsymbol{r}) = \Phi_{00}^{1}(\boldsymbol{r}),$$

where

$$\Phi_{FM}^{L}(\boldsymbol{r}) = R_F^L(r) \sum_\sigma [\mathsf{Y}_{FM}^L(\boldsymbol{r})]^\sigma \mathsf{e}_\sigma, \quad [\mathsf{Y}_{FM}^L(\boldsymbol{r})]^\sigma = C_{L,M-\sigma,1,\sigma}^{FM} Y_{FM-\sigma}(\boldsymbol{r}/r), \tag{A1.5}$$

e_σ are the covariant cyclic orts composed of the Bloch functions, $C_{L,M-\sigma,1,\sigma}^{F,M}$ are the Clebsch-Gordan coefficients, and $Y_{FM-\sigma}(\boldsymbol{r}/r)$ denote the corresponding spherical harmonics.[45] In the basis of $(\mathsf{e}_1, \mathsf{e}_0, \mathsf{e}_{-1})$ we get

$$\mathsf{K}_x = (i/\sqrt{2}) \begin{pmatrix} 0 & -1 & 0 \\ 1 & 0 & 1 \\ 0 & -1 & 0 \end{pmatrix}, \mathsf{K}_y = (1/\sqrt{2}) \begin{pmatrix} 0 & 1 & 0 \\ 1 & 0 & -1 \\ 0 & -1 & 0 \end{pmatrix}, \mathsf{K}_z = i \begin{pmatrix} 0 & 0 & -1 \\ 0 & 0 & 0 \\ 1 & 0 & 0 \end{pmatrix}. \tag{A1.6}$$

Therefore, we arrive at the following expressions for the solutions of type hm:

$$\Psi_{FF_z}^{hm,\dagger} \mathsf{K}_x \Psi_{FF_z}^{hm} = i \sum_{L_1,L_2=F\pm1} \sum_{M_1,M_2=F_z,F_z\pm1:\, M_1-M_2=1} \Lambda_{FL_1M_1}^*(\boldsymbol{r}) \Lambda_{FL_2M_2}(\boldsymbol{r}) + c.c., \tag{A1.7}$$

$$\Psi_{FF_z}^{hm,\dagger} \mathsf{K}_y \Psi_{FF_z}^{hm} = \sum_{L_1,L_2=F\pm1} \sum_{M_1,M_2=F_z,F_z\pm1:\, M_1-M_2=1} \Lambda_{L_1M_1}^*(\boldsymbol{r}) \Lambda_{L_2M_2}(\boldsymbol{r}) + c.c.,$$

$$\Psi_{FF_z}^{hm,\dagger} \mathsf{K}_z \Psi_{F,F_z}^{hm} = i \sum_{L_1,L_2=F\pm1} \Lambda_{F,L_1,F_z-1}^*(\boldsymbol{r}) \Lambda_{F,L_2,F_z+1}(\boldsymbol{r}) + c.c.; \tag{A1.8}$$

whereas, for the solutions of type hh, one obtains

$$\Psi_{FF_z}^{hh,\dagger} \mathsf{K}_x \Psi_{FF_z}^{hh} = i \Lambda_{F,F,F_z-1}^*(\boldsymbol{r}) \Lambda_{F,F,F_z}(\boldsymbol{r}) + i \Lambda_{F,F,F_z}^*(\boldsymbol{r}) \Lambda_{F,F,F_z+1}(\boldsymbol{r}) + c.c.,$$

$$\Psi_{FF_z}^{hh,\dagger} \mathsf{K}_y \Psi_{FF_z}^{hh} = -\Lambda_{F,F,F_z-1}^*(\boldsymbol{r}) \Lambda_{F,F,F_z}(\boldsymbol{r}) - \Lambda_{F,F,F_z}^*(\boldsymbol{r}) \Lambda_{F,F,F_z+1}(\boldsymbol{r}) + c.c.,$$

$$\Psi_{FF_z}^{hh,\dagger} \mathsf{K}_z \Psi_{FF_z}^{hh} = i \Lambda_{F,F,F_z-1}^*(\boldsymbol{r}) \Lambda_{F,F,F_z+1}(\boldsymbol{r}) + c.c.; \tag{A1.9}$$

and, finally, for the solutions of type hl, one gets

$$\Psi_{F_z}^{hl,\dagger} \mathsf{K}_x \Psi_{F_z}^{hl} = i \sum_{M_1,M_2=F_z,F_z\pm1:\, M_1-M_2=1} \Lambda_{0,1,M_1}^*(\boldsymbol{r}) \Lambda_{0,1,M_2}(\boldsymbol{r}) + c.c.,$$

$$\Psi_{F_z}^{hl,\dagger} \mathsf{K}_y \Psi_{F_z}^{hl} = \sum_{M_1,M_2=F_z,F_z\pm1:\, M_1-M_2=1} \Lambda_{0,1,M_1}^*(\boldsymbol{r}) \Lambda_{0,1,M_2}(\boldsymbol{r}) + c.c.,$$

$$\Psi_{F_z}^{hl,\dagger} \mathsf{K}_z \Psi_{F_z}^{hl} = i \Lambda_{0,1,F_z-1}^*(\boldsymbol{r}) \Lambda_{0,1,F_z+1}(\boldsymbol{r}) + c.c.. \tag{A1.10}$$

For the optical-phonon transition matrix elements between the hh and hm states (nonadiabatics) we get

$$\Psi^{hh,\dagger}_{FF_z}\mathsf{K}_x\Psi^{hm}_{F'F'_z} = \mathrm{i}\sum_{L'=F'\pm1}\sum_{M=0,1}\left[\Lambda^*_{F,F,F_z-1+M}(\boldsymbol{r})\,\Lambda_{F',L',F'_z+M}(\boldsymbol{r}) - \Lambda^*_{F,F,F_z-1-M}(\boldsymbol{r})\,\Lambda_{F',L',F'_z-M}(\boldsymbol{r})\right],$$

$$\Psi^{hh,\dagger}_{FF_z}\mathsf{K}_y\Psi^{hm}_{F'F'_z} = -\sum_{L'=F'\pm1}\sum_{M=0,1}\left[\Lambda^*_{F,F,F_z-1+M}(\boldsymbol{r})\,\Lambda_{F',L',F'_z+M}(\boldsymbol{r}) + \Lambda^*_{F,F,F_z-1-M}(\boldsymbol{r})\,\Lambda_{F',L',F'_z-M}(\boldsymbol{r})\right],$$

$$\Psi^{hh,\dagger}_{FF_z}\mathsf{K}_z\Psi^{hm}_{F'F'_z} = \mathrm{i}\sum_{L'=F'\pm1}\left[\Lambda^*_{F,F,F_z-1}(\boldsymbol{r})\,\Lambda_{F',L',F'_z+1}(\boldsymbol{r}) - \Lambda^*_{F,F,F_z+1}(\boldsymbol{r})\,\Lambda_{F',L',F'_z-1}(\boldsymbol{r})\right]. \tag{A1.11}$$

The functions Λ introduced above are related to the contravariant cyclic components of the vectors $\boldsymbol{\Phi}$ given by (A1.5) as follows

$$\Lambda_{F,L,M\mp1} = \mp[\Phi^L_{FM}]^{\pm1}, \quad \Lambda_{F,L,M} = [\Phi^L_{FM}]^0/\sqrt{2}. \tag{A1.12}$$

Appendix 2.

The matrices $\mathsf{H}^{\hat{q}}_\nu$ can be found from Eq. (12) after substitution of the polarization vectors (A1.2):

$$\mathsf{H}^{\hat{q}}_L = \begin{pmatrix} a + \dfrac{b}{6}(3\cos^2\theta - 1) & \dfrac{b}{2\sqrt{2}}\sin 2\theta e^{-\mathrm{i}\varphi} & b\dfrac{\sin^2\theta}{2}e^{-2\mathrm{i}\varphi} \\[2mm] \dfrac{b}{2\sqrt{2}}\sin 2\theta e^{\mathrm{i}\varphi} & a - \dfrac{b}{3}(3\cos^2\theta - 1) & -\dfrac{b}{2\sqrt{2}}\sin 2\theta e^{-\mathrm{i}\varphi} \\[2mm] b\dfrac{\sin^2\theta}{2}e^{2\mathrm{i}\varphi} & -\dfrac{b}{2\sqrt{2}}\sin 2\theta e^{\mathrm{i}\varphi} & a + \dfrac{b}{6}(3\cos^2\theta - 1) \end{pmatrix}, \tag{A2.1}$$

$$\mathsf{H}^{\hat{q}}_{T_1} = \frac{b}{2}\begin{pmatrix} 0 & \dfrac{\mathrm{i}}{2\sqrt{2}}\sin 2\theta e^{-\mathrm{i}\varphi} & \mathrm{i}\sin^2\theta e^{-2\mathrm{i}\varphi} \\[2mm] -\dfrac{\mathrm{i}}{2\sqrt{2}}\sin 2\theta e^{\mathrm{i}\varphi} & 0 & -\dfrac{\mathrm{i}}{2\sqrt{2}}\sin 2\theta e^{-\mathrm{i}\varphi} \\[2mm] -\mathrm{i}\sin^2\theta e^{2\mathrm{i}\varphi} & \dfrac{\mathrm{i}}{2\sqrt{2}}\sin 2\theta e^{\mathrm{i}\varphi} & 0 \end{pmatrix}, \tag{A2.2}$$

$$\mathsf{H}^{\hat{q}}_{T_2} = \frac{b}{2}\begin{pmatrix} -\dfrac{1}{2}\sin 2\theta & \dfrac{1}{\sqrt{2}}\cos 2\theta e^{-\mathrm{i}\varphi} & \sin(2\theta)e^{-2\mathrm{i}\varphi} \\[2mm] \dfrac{1}{\sqrt{2}}\cos 2\theta e^{\mathrm{i}\varphi} & \sin 2\theta & -\dfrac{1}{\sqrt{2}}\cos 2\theta e^{-\mathrm{i}\varphi} \\[2mm] \sin(2\theta)e^{2\mathrm{i}\varphi} & -\dfrac{1}{\sqrt{2}}\cos 2\theta e^{\mathrm{i}\varphi} & -\dfrac{1}{2}\sin 2\theta \end{pmatrix}, \tag{A2.3}$$

where θ and φ are, respectively, the polar and the azimuthal angles of the vector $\boldsymbol{q}$.

Appendix 3.

Here we discuss the derivation of Eq. (36) for the effective Huang-Rhys factor accounting for the multiphonon transitions between the degenerate hole levels. We use the Hamiltonian (4) and write the hole wave function as

$$\hat{\Psi}(t) = \left[\sum_{M_2}\hat{v}_{M_2}(t)c^\dagger_{2,M_2} + \sum_{M_1}\hat{w}_{M_1}(t)c^\dagger_{1,M_1}\right]|0\rangle \tag{A3.1}$$

where $|0\rangle$ is the hole vacuum and $\hat{v}_{M_2}(t)$, $\hat{w}_{M_1}(t)$ are the operators acting on the phonon subsystem. Here the index M_i runs over values $-F_i,\ldots,F_i$ ($i=1,2$). The wave function (A3.1) satisfies the system of equations [following from the Schrödinger equation written in the interaction representation with respect to the free-phonon part of the Hamiltonian (8)]:

$$\mathrm{i}\hbar\frac{d\hat{v}_{M_2}}{dt} = \varepsilon_2\hat{v}_{M_2} + \sum_{M'_2}\widetilde{H}^{M_2M'_2}_{2,\mathrm{opt}}\hat{v}_{M'_2},$$

$$\mathrm{i}\hbar\frac{d\hat{w}_{M_1}}{dt} = \varepsilon_1\hat{w}_{M_1} + \sum_{M'_1}\widetilde{H}^{M_1M'_1}_{1,\mathrm{opt}}\hat{w}_{M'_1} + \sum_{M'_2}\widetilde{H}^{M_1M'_2}_{2\to1,\mathrm{ac}}\hat{v}_{M'_2},$$

$$\tag{A3.2}$$

where

$$\widetilde{H}_{i,\text{opt}}^{M_iM_i'} = \sum_{\boldsymbol{q},\boldsymbol{\nu}} \left[V_{i,\boldsymbol{q\nu}}^{M_iM_i'} b_{\boldsymbol{q\nu}} e^{-\mathrm{i}\omega_{\boldsymbol{q\nu}}t} + (V_{i,\boldsymbol{q\nu}}^{M_i'M_i})^* b_{\boldsymbol{q\nu}}^\dagger e^{\mathrm{i}\omega_{\boldsymbol{q\nu}}t} \right],$$

$$H_{2\to1,\text{ac}}^{M_1M_2'} = \sum_{\boldsymbol{k},\boldsymbol{\nu}} \left[V_{12,\boldsymbol{k\nu}}^{M_1M_2'} a_{\boldsymbol{k\nu}} e^{-\mathrm{i}s_\nu kt} + (V_{12,\boldsymbol{k\nu}}^{M_2'M_1})^* a_{\boldsymbol{k\nu}}^\dagger e^{\mathrm{i}s_\nu kt} \right].$$

The initial conditions for the system (A3.2) are

$$\hat{v}_{M_2}(t=0)=1, \quad \hat{v}_{M_2'}(t=0)=\hat{w}_{M_1}(t=0)=0, \quad M_2' \neq M_2,$$
$$(A3.3)$$

in the case when the state $|2, M_2\rangle$ is initially populated. The relaxation rate is given by

$$W(M_2) = \lim_{t\to\infty} \frac{1}{t} \left[\sum_{M_1} \langle\langle \hat{w}_{M_1}^\dagger(t)\hat{w}_{M_1}(t) \rangle\rangle \right], \quad (A3.4)$$

where the double angular brackets denote averaging over the thermal distribution of the phonon states. The probability averaged over the multiplet of the possible initial hole states is given by

$$W = \frac{1}{2F_2+1} \sum_{M_2} W(M_2). \quad (A3.5)$$

For a given number p of emitted optical phonons one can employ a perturbation theory to find the transition probability W_p (cf. Sec. III, B). Let us consider the case when exactly one optical and one acoustic phonons are emitted. For non-degenerate levels one would get

$$W_1 = \frac{1}{\tau_{\text{ac}}}(N_{\hbar\omega_{\text{opt}}} + 1)S, \quad (A3.6)$$

i.e. the result is proportional to the Huang-Rhys factor S.

Generalization of Eq. (A3.6) for the case of the degenerate initial and final levels leads to the following expression

$$W_1 = \frac{2\pi}{\omega_{\text{opt}}^2\hbar^3}(N_{\hbar\omega_{\text{opt}}} + 1)\frac{1}{2F_2+1}$$
$$\times \sum_{M_1,M_2} \sum_{\boldsymbol{q},\boldsymbol{\nu}} \sum_{\boldsymbol{k},\boldsymbol{\eta}} \left| \mathcal{M}_{\boldsymbol{q\nu},\boldsymbol{k\eta}}^{M_1M_2} \right|^2 \quad (A3.7)$$
$$\times (N_{\hbar s_\eta k} + 1)\delta(\varepsilon_2 - \varepsilon_1 - \hbar\omega_{\text{opt}} - \hbar s_\eta k),$$

where

$$\mathcal{M}_{\boldsymbol{q\nu},\boldsymbol{k\eta}}^{M_1M_2} = \sum_{M_1'} V_{1,\boldsymbol{q\nu}}^{M_1M_1'} V_{12,\boldsymbol{k\eta}}^{M_1'M_2} - \sum_{M_2'} V_{12,\boldsymbol{k\eta}}^{M_1M_2'} V_{2,\boldsymbol{q\nu}}^{M_2'M_2}. \quad (A3.8)$$

We would like to stress that the transition probability is determined by a superposition of the two distinct processes with different intermediate virtual states: $|2, M_2\rangle \xrightarrow{\hbar\omega_{\text{ac}}} |1, M_1'\rangle \xrightarrow{\hbar\omega_{\text{opt}}} |1, M_1\rangle$ and $|2, M_2\rangle \xrightarrow{\hbar\omega_{\text{opt}}} |2, M_2'\rangle \xrightarrow{\hbar\omega_{\text{ac}}} |1, M_1\rangle$.

We proceed by diagonalizing the Hamiltonians (5) for each optical phonon mode $(\boldsymbol{q}, \boldsymbol{\nu})$ and find the corresponding eigenstates $|1, \widetilde{M}_1(\boldsymbol{q}, \boldsymbol{\nu})\rangle$ and $|2, \widetilde{M}_2(\boldsymbol{q}, \boldsymbol{\nu})\rangle$ such that

the matrices $V_{i,\boldsymbol{q\nu}}^{\widetilde{M}_2(\boldsymbol{q},\boldsymbol{\nu})\widetilde{M}_2'(\boldsymbol{q},\boldsymbol{\nu})}$ become diagonal. To simplify notations we omit the indices $(\boldsymbol{q}, \boldsymbol{\nu})$ in the superscripts. In the new basis the matrix (A3.8) takes the form

$$\mathcal{M}_{\boldsymbol{q\nu},\boldsymbol{k\eta}}^{\widetilde{M}_1\widetilde{M}_2} = V_{12,\boldsymbol{k\eta}}^{\widetilde{M}_1\widetilde{M}_2} \left(V_{1,\boldsymbol{q\nu}}^{\widetilde{M}_1\widetilde{M}_1} - V_{2,\boldsymbol{q\nu}}^{\widetilde{M}_2\widetilde{M}_2} \right). \quad (A3.9)$$

In order to decouple the acoustic phonon and the optical phonon contributions we replace $V_{i,\boldsymbol{q\nu}}^{\widetilde{M}_i\widetilde{M}_i}$ by its value averaged over the multiplet:

$$V_{i,\boldsymbol{q\nu}} = \frac{1}{2F_i+1} \sum_{\widetilde{M}_i} V_{i,\boldsymbol{q\nu}}^{\widetilde{M}_i\widetilde{M}_i}. \quad (A3.10)$$

This leads to the following expression

$$\mathcal{M}_{\boldsymbol{q\nu},\boldsymbol{k\eta}}^{\widetilde{M}_1\widetilde{M}_2} = V_{12,\boldsymbol{k\eta}}^{\widetilde{M}_1\widetilde{M}_2} \left(V_{1,\boldsymbol{q\nu}} - V_{2,\boldsymbol{q\nu}} \right). \quad (A3.11)$$

As a result, we achieve factorization of the matrix element in Eq. (A3.7):

$$\frac{1}{2F_2+1} \sum_{\widetilde{M}_1,\widetilde{M}_2} \left| \mathcal{M}_{\boldsymbol{q\nu},\boldsymbol{k\eta}}^{\widetilde{M}_1\widetilde{M}_2} \right|^2 = |V_{1,\boldsymbol{q\nu}} - V_{2,\boldsymbol{q\nu}}|^2$$
$$\times \frac{1}{2F_2+1} \sum_{\widetilde{M}_1,\widetilde{M}_2} \left| V_{12,\boldsymbol{k\eta}}^{\widetilde{M}_1\widetilde{M}_2} \right|^2. \quad (A3.12)$$

This expression is invariant under the basis transformations for both the initial and the final hole multiplets. In particular, these basis states may be chosen to be independent of the phonon mode. Finally, we arrive at the result

$$W_1 = \frac{1}{\tau_{\text{ac}}}(N_{\hbar\omega_{\text{opt}}} + 1)S_{\text{av}}, \quad (A3.13)$$

where S_{av} is given by Eq. (36) and $1/\tau_{\text{ac}}$ is given by Eq. (38). Comparing Eq. (A3.13) to Eq. (A3.6) one can identify S_{av} with an effective Huang-Rhys factor for multiphonon transitions between the hole multiplets.

Appendix 4.

Generally, V_p is given by the sum of $p + 1$ terms, describing the interference between the Hamiltonians $\widetilde{H}_i^{(\text{opt})}$ and $\widetilde{H}_f^{(\text{opt})}$,

$$V_p = \frac{1}{(\hbar\omega_{\text{opt}})^p} \sum_{\boldsymbol{q}_1,\boldsymbol{q}_2...\boldsymbol{q}_p} \sum_{m=0}^{p} \frac{(-1)^m}{p!(m-p)!}$$
$$\times \underbrace{b_{\boldsymbol{q}_1}^{(2\to1)\dagger} b_{\boldsymbol{q}_2}^{(1\to2)\dagger} \dots b_{\boldsymbol{q}_p}^{(j\to3-j)\dagger}}_{p \text{ factors}}$$
$$\times \underbrace{B_{i,\boldsymbol{q}_1} \dots B_{i,\boldsymbol{q}_m}^*}_{m \text{ factors}} \underbrace{B_{f,\boldsymbol{q}_{m+1}} \dots B_{f,\boldsymbol{q}_p}^*}_{p-m \text{ factors}}.$$
$$(A4.14)$$

It is instructive to analyze the cases when $p = 1, 2$ and Eq. (A4.14) can be presented in a compact form. For $p = 1$ the value of V_p is obtained by a single iteration over the Hamiltonians $\widetilde{H}_{i,f}^{(\mathrm{opt})}$:

$$V_1 = \frac{1}{\hbar\omega_{\mathrm{opt}}} \sum_{\boldsymbol{q}} b_{\boldsymbol{q}}^{(2\to1)\dagger} (B_{i,\boldsymbol{q}} - B_{f,\boldsymbol{q}}) . \qquad (A4.15)$$

The two terms in Eq. (A4.15) stem from the diagonal electron-phonon interaction in the initial and the final states. These two channels of relaxation are schematically illustrated in Figs. 7(a) and 7(b): an electron can either subsequently emit one optical and one acoustic phonon or vice versa. The correlator $\langle V_1^\dagger V_1 \rangle$ is given by

$$\langle V_1^\dagger V_1 \rangle = \frac{N_{\hbar\omega_{\mathrm{opt}}} + 1}{(\hbar\omega_{\mathrm{opt}})^2} \sum_{\boldsymbol{q}} |B_{i,\boldsymbol{q}} - B_{f,\boldsymbol{q}}|^2 . \qquad (A4.16)$$

Using the identity

$$\int \frac{\mathrm{d}^3 q}{(2\pi)^3} \left| \int \mathrm{d}^3 r f(\boldsymbol{r}) e^{\mathrm{i}\boldsymbol{qr}} \right|^2 = \int \mathrm{d}^3 r |f(\boldsymbol{r})|^2 \qquad (A4.17)$$

we recast Eq. (A4.16) as

$$\langle V_1^\dagger V_1 \rangle = (N_{\hbar\omega_{\mathrm{opt}}} + 1)\sigma_{\mathrm{e}}\tilde{\alpha}_{\mathrm{i}\to f}(p = 1) , \qquad (A4.18)$$

where $\tilde{\alpha}_{\mathrm{i}\to f}(p = 1)$ is given by

$$\tilde{\alpha}_{\mathrm{i}\to f}(p = 1) \equiv \mathcal{S} = R^3 \int \mathrm{d}^3 r (|\psi_i(\boldsymbol{r})|^2 - |\psi_f(\boldsymbol{r})|^2)^2 . \qquad (A4.19)$$

This expression is exactly the same as in the single valley case, with the Huang-Rhys factor $S = \sigma_{\mathrm{e}}\mathcal{S}$, since the relaxation process shown in Fig. 7 involves only one of the two types of intervalley phonons. A more interesting case is realized for $p = 2$, when two intervalley phonons are emitted. The three possible relaxation channels for $p = 2$ are illustrated in Fig. 8. They are described by

$$V_2 = \frac{1}{2(\hbar\omega_{\mathrm{opt}})^2} \sum_{\boldsymbol{q},\boldsymbol{q}'} b_{\boldsymbol{q}}^{(2\to1)\dagger} b_{\boldsymbol{q}'}^{(1\to2)\dagger}$$
$$\times (B_{i,\boldsymbol{q}} B_{i,\boldsymbol{q}'}^* - 2 B_{i,\boldsymbol{q}} B_{f,\boldsymbol{q}'}^* + B_{f,\boldsymbol{q}} B_{f,\boldsymbol{q}'}^*) . \qquad (A4.20)$$

so that the result can be expressed in powers of $\mathcal{S}$. The correlator $\langle V_2^\dagger V_2 \rangle$ is calculated using the identity

$$\langle b_{\boldsymbol{q}}^{(2\to1)} b_{\boldsymbol{q}'}^{(1\to2)} b_{\boldsymbol{k}}^{(2\to1)\dagger} b_{\boldsymbol{k}'}^{(1\to2)\dagger} \rangle = (N_{\hbar\omega_{\mathrm{opt}}} + 1)^2 \delta_{\boldsymbol{k},\boldsymbol{q}} \delta_{\boldsymbol{k}',\boldsymbol{q}'} . \qquad (A4.21)$$

The result reads

$$\langle V_2^\dagger V_2 \rangle = (N_{\hbar\omega_{\mathrm{opt}}} + 1)^2 \sigma_{\mathrm{e}}^2 \tilde{\alpha}_{\mathrm{i}\to f}(p = 2) . \qquad (A4.22)$$

Here

$$\tilde{\alpha}_{\mathrm{i}\to f}(p = 2) \equiv \frac{1}{4}(\mathcal{S}^2 + 2\mathcal{S}\mathcal{U} - 2\mathcal{C}^2) , \qquad (A4.23)$$
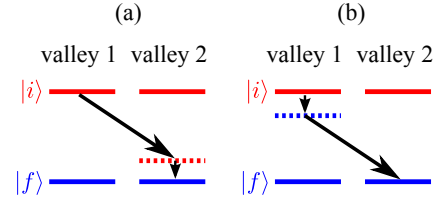

FIG. 7. Schematic illustration of relaxation processes with emission of one optical and one acoustic phonons, contributing to Eq. (A4.15). Inclined and vertical lines indicate intervalley optical and intravalley acoustic phonons, respectively.
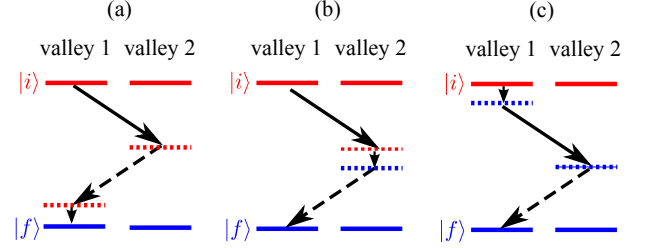

FIG. 8. Schematic illustration of relaxation processes with emission of two optical and one acoustic phonons, contributing to Eq. (A4.20). Inclined and vertical lines indicate intervalley optical and intravalley acoustic phonons, respectively.

while the integrals $\mathcal{U}$ and $\mathcal{C}$ are given by

$$\mathcal{U} = R^3 \int \mathrm{d}^3 r |\psi_i(\boldsymbol{r})|^4 , \qquad (A4.24)$$

$$\mathcal{C} = R^3 \int \mathrm{d}^3 r |\psi_i(\boldsymbol{r})|^2 (|\psi_f(\boldsymbol{r})|^2 - |\psi_i(\boldsymbol{r})|^2) . \qquad (A4.25)$$

Equation (A4.23) is different from the simple single-valley expression $\mathcal{S}^2/2!$, because both types of phonons are involved in the transition. Indeed, in the single-valley case, when $b_{\boldsymbol{q}}^{(2\to1)} \equiv b_{\boldsymbol{q}'}^{(1\to2)} \equiv b_{\boldsymbol{q}}$, Eq. (A4.20) can be factorized:

$$V_2 = \frac{1}{2(\hbar\omega_{\mathrm{opt}})^2} \sum_{\boldsymbol{q}} b_{\boldsymbol{q}}^\dagger (B_{i,\boldsymbol{q}} - B_{f,\boldsymbol{q}}) \times \sum_{\boldsymbol{q}'} b_{\boldsymbol{q}'}^\dagger (B_{i,\boldsymbol{q}'}^* - B_{f,\boldsymbol{q}'}^*) . \qquad (A4.26)$$

We have also obtained the quantities

$$\langle V_p^\dagger V_p \rangle = (N_{\hbar\omega_{\mathrm{opt}}} + 1)^p \sigma_{\mathrm{e}}^p \tilde{\alpha}_{\mathrm{i}\to f}(p) \qquad (A4.27)$$

for $p = 3 \ldots 5$. For $p = 3$ the factor $\tilde{\alpha}_{\mathrm{i}\to f}$ is given by

$$\tilde{\alpha}_{\mathrm{i}\to f}(p = 3) = \frac{1}{3}\mathcal{S}\mathcal{U}^2 - \frac{1}{3}\mathcal{U}\mathcal{C}^2 + \frac{1}{3}\mathcal{U}\mathcal{C}\mathcal{S} - \frac{1}{3}\mathcal{C}^3$$
$$- \frac{1}{12}\mathcal{C}^2\mathcal{S} + \frac{1}{12}\mathcal{S}^2\mathcal{U} + \frac{1}{18}\mathcal{S}^3 . \qquad (A4.28)$$

The cases of $p = 4, 5$ are also trivial but the results are too cumbersome to be given here. It is worth to note, however, that the factor $\tilde{\alpha}_{\mathrm{i}\to f}(p)$ can be always presented in powers of the integrals $\mathcal{U}, \mathcal{S}$, and $\mathcal{C}$.

The relaxation process considered above is similar to that studied in Ref. [18]. In the latter work the virtual intermediate states for the multiphonon transitions originated from the levels of the size quantization different from the initial and the final levels. In our case the virtual intermediate electron states originate from different valleys but are characterized by the same envelope functions as the initial or the final states.

* andrey.moskalenko@physik.uni-halle.de

† poddubny@coherent.ioffe.ru

[1] L. Pavesi, L. Dal Negro, C. Mazzoleni, G. Franzo, and F. Priolo, Nature (London) **408**, 440 (2000).

[2] A. Polman, Nat. Materials **1**, 10 (2002).

[3] I. Izeddin, A. S. Moskalenko, I. N. Yassievich, M. Fujii, and T. Gregorkiewicz, Phys. Rev. Lett. **97**, 207401 (2006).

[4] D. Timmerman, I. Izeddin, P. Stallinga, I. N. Yassievich, and T. Gregorkiewicz, Nat. Photonics **2**, 105 (2008).

[5] W. D. A. M. de Boer, D. Timmerman, K. Dohnalova, I. N. Yassievich, H. Zhang, W. J. Buma, and T. Gregorkiewicz, Nat. Nanotechnology **5**, 878 (2010).

[6] C. Delerue and M. Lannoo, eds., *Nanostructures: Theory and Modelling* (Springer-Verlag, Berlin, 2004).

[7] L. Pavesi and R. Turan, eds., *Silicon Nanocrystals: Fundamentals, Synthesis and Applications* (Wiley-VCH, Weinheim, 2010).

[8] A. A. Prokofiev, A. S. Moskalenko, I. N. Yassievich, W. D. A. M. de Boer, D. Timmerman, H. Zhang, W. J. Buma, and T. Gregorkiewicz, JETP Lett. **90**, 758 (2009).

[9] F. Trojánek, K. Neudert, M. Bittner, and P. Malý, Phys. Rev. B **72**, 075365 (2005).

[10] J. Valenta, A. Fucikova, I. Pelant, K. Kusova, K. Dohnalova, A. Aleknavicius, O. Cibulka, A. Fojtik, and G. Kada, New J. Phys. **10**, 073022 (2008).

[11] A. N. Poddubny, A. A. Prokofiev, and I. N. Yassievich, Appl. Phys. Lett. **97**, 231116 (2010).

[12] I. Mihalcescu, J. C. Vial, A. Bsiesy, F. Muller, R. Romestain, E. Martin, C. Delerue, M. Lannoo, and G. Allan, Phys. Rev. B **51**, 17605 (1995).

[13] C. Delerue, M. Lannoo, G. Allan, E. Martin, I. Mihalcescu, J. C. Vial, R. Romestain, F. Muller, and A. Bsiesy, Phys. Rev. Lett. **75**, 2228 (1995).

[14] A. N. Poddubny, A. S. Moskalenko, A. A. Prokofiev, S. V. Goupalov, and I. N. Yassievich, Phys. Status Solidi C **8**, 985 (2011).

[15] C. Jacoboni and L. Reggiani, Rev. Mod. Phys. **55**, 645 (1983).

[16] T. Kunikiyo, M. Takenaka, Y. Kamakura, M. Yamaji, H. Mizuno, M. Morifuji, K. Taniguchi, and C. Hamaguchi, J. Appl. Phys. **75**, 297 (1994).

[17] Y. Kamakura, I. Kawashima, K. Deguchi, and K. Taniguchi, J. Appl. Phys. **88**, 5802 (2000).

[18] T. Inoshita and H. Sakaki, Phys. Rev. B **46**, 7260 (1992).

[19] S. V. Goupalov, Phys. Rev. B **72**, 073301 (2005).

[20] R. D. Schaller, J. M. Pietryga, S. V. Goupalov, M. A. Petruska, S. A. Ivanov, and V. I. Klimov, Phys. Rev. Lett. **95**, 196401 (2005).

[21] A. Pandey and P. Guyot-Sionnest, Science **322**, 929 (2008).

[22] V. N. Stavrou and X. Hu, Phys. Rev. B **73**, 205313 (2006).

[23] A. A. Prokofiev, S. V. Goupalov, A. S. Moskalenko, A. N. Poddubny, and I. N. Yassievich, Physica E **41**, 969 (2009).

[24] B. Delley and E. F. Steigmeier, Phys. Rev. B **47**, 1397 (1993).

[25] C. Garoufalis and A. Zdetsis, Phys. Chem. Chem. Phys. **8**, 808 (2006).

[26] M. Luppi and S. Ossicini, Phys. Rev. B **71**, 035340 (2005).

[27] E. Luppi, F. Iori, R. Magri, O. Pulci, S. Ossicini, E. Degoli, and V. Olevano, Phys. Rev. B **75**, 033303 (2007).

[28] Y. M. Niquet, C. Delerue, G. Allan, and M. Lannoo, Phys. Rev. B **62**, 5109 (2000).

[29] L.-W. Wang and A. Zunger, J. Chem. Phys. **100**, 2394 (1994).

[30] S. Ogut, J. R. Chelikowsky, and S. G. Louie, Phys. Rev. Lett. **79**, 1770 (1997).

[31] A. S. Moskalenko, J. Berakdar, A. A. Prokofiev, and I. N. Yassievich, Phys. Rev. B **76**, 085427 (2007).

[32] V. N. Abakumov, V. I. Perel, and I. N. Yassievich, *Nonradiative Recombination in Semiconductors*, Modern Problems in Condensed Matter Sciences Vol. 33, edited by V. M. Agranovich and A. A. Maradudin (Elsevier, Amsterdam, 1991).

[33] P. Yu and M. Cardona, *Fundamentals of Semiconductors - Physics and Materials Properties (3rd Edition)* (Springer, Berlin, 2001).

[34] W. Jantsch and Z. Wilamowski, in *Spin Physics in Semiconductors*, edited by M. Dyakonov (Springer, Berlin, 2008) pp. 179–210.

[35] S. P. Dash, S. Sharma, R. S. Patel, M. P. de Jong, and R. Jansen, Nature (London) **462**, 491 (2009).

[36] D. J. Lepine, Phys. Rev. B **6**, 436 (1972).

[37] J. L. Cheng, M. W. Wu, and J. Fabian, Phys. Rev. Lett. **104**, 016601 (2010).

[38] X. Hu and J. Zi, J. Phys.: Cond. Matter **14**, L671 (2002).

[39] A. Valentin, J. Se, S. Galdin-Retailleau, and P. Dollfus, J. Phys.: Cond. Matter **20**, 145213 (2008).

[40] L. Donetti, F. Gámiz, J. B. Roldán, and A. Godoy, J. Appl. Phys. **100**, 013701 (2006).

[41] K. Huang and A. Rhys, Proc. Roy. Soc. London A **204**, 406 (1950).

[42] K. Huang, Scientia Sinica **24**, 27 (1981).

[43] G. L. Bir and G. E. Pikus, *Symmetry and Strain-Induced Effects in Semiconductors* (Nauka, Moscow, 1972).

[44] B. K. Ridley, *Quantum Processes in Semiconductors* (Clarendon, Oxford, 1999).

[45] D. A. Varshalovich, A. N. Moskalev, and V. K. Khersonskii, *Quantum Theory of Angular Momentum* (World Scientific, Singapore, 1988).

[46] A. Dargys and J. Kundrotas, *Handbook on physical properties of Ge, Si, GaAs, and InP* (Science and Encyclopedia Publishers, Vilnius, 1994).

[47] L. Brey, N. E. Christensen, and M. Cardona, Phys. Rev. B **36**, 2638 (1987).

[48] A. Blacha, H. Presting, and M. Cardona, Phys. Status Solidi B **126**, 11 (1984).

[49] A. S. Ioselevich and E. I. Rashba, *Theory of nonradiative transitions*, Quantum Tunneling in Condensed Media, Modern Problems in Condensed Matter Sciences Vol. 34, edited by Y. M. Kagan and A. J. Leggett (Elsevier, Amsterdam, 1992).

[50] In the case of GaAs the corresponding matrix element is proportional to q because of the different type of the dominating electron interaction with optical phonons, which is of the Fröhlich type there. For GaAs NCs, the transition rates drops by several orders of magnitudes by the phonon energy deviation of just 20-30 μeV. The corresponding energy range for Si NCs is larger than these extreme small values.

[51] C. P. Lindsey and G. D. Patterson, J. Chem. Phys. **73**, 3348 (1980).

[52] M. Shlesinger, J. Stat. Phys. **36**, 639 (1984).

[53] C. Delerue, G. Allan, C. Reynaud, O. Guillois, G. Ledoux,

and F. Huisken, Phys. Rev. B **73**, 235318 (2006).

[54] W. Zhang, C. Delerue, Y.-M. Niquet, G. Allan, and E. Wang, Phys. Rev. B **82**, 115319 (2010).

[55] V. Burdov, Semiconductors **36**, 1154 (2002).

[56] S. M. Sze, *Physics of Semiconductor Devices* (J. Wiley & Sons, New York, 1981).

[57] Z. A. Weinberg, J. Appl. Phys. **53**, 5052 (1982).

[58] A. Puzder, A. J. Williamson, J. C. Grossman, and G. Galli, Phys. Rev. Lett. **88**, 097401 (2002).

[59] H. W. Streitwolf, Phys. Status Solidi B **37**, K47 (1970).

[60] M. Lax and J. L. Birman, Phys. Status Solidi B **49**, K153 (1972).

[61] D. Long, Phys. Rev. **120**, 2024 (1960).

[62] D. K. Ferry, Phys. Rev. B **14**, 1605 (1976).

[63] C. M. Krowne and J. W. Holm-Kennedy, Surf. Sci. **46**, 197 (1974).

[64] S. Sinha, P. K. Schelling, S. R. Phillpot, and K. E. Goodson, J. Appl. Phys. **97**, 023702 (2005).

[65] M. Asche and O. G. Sarbei, Phys. Status Solidi B **103**, 11 (1981).

[66] L. I. Glazman and R. I. Shekhter, Sov. Phys. JETP **67**, 163 (1988).

[67] We have included up to five emitted optical phonons in our numerical calculation.

[68] A. Poddubny, S. Goupalov, V. Kozub, and I. Yassievich, JETP Lett. **90**, 683 (2010).

[69] G. Allan and C. Delerue, Phys. Rev. B **79**, 195324 (2009).